Department of Precision and Microsystems Engineering

Influence of Mode-Coupling on Q-factor in Nanomechanical Resonators

M.A. ten Wolde

Report no : 2021.029
Coach : Dr. R.A. Norte and Ir. M.H.J. de Jong
Professor : Prof. Dr. Ir. P.G. Steeneken
Specialisation : Dynamics of Micro- and Nanosystems
Type of report : Master thesis
Date : May 10$^{\text{th}}$, 2021

Delft
University of
Technology

Challenge the future

TU DELFT

MASTER OF SCIENCE THESIS

Influence of Mode-Coupling on Q-factor in Nanomechanical Resonators

---

Author:
M.A. TEN WOLDE
4757769

Supervisors:
Dr. R.A. NORTE
Prof. Dr. Ir. P.G. STEENEKEN
Ir. M. H. J. DE JONG

A thesis submitted in fulfillment of the requirements
for the degree of Master of Science in Mechanical Engineering

in the

Dynamics of Micro and Nanosystems Group
Department of Precision and Microsystems Engineering

May 9, 2021

"Nobody ever figures out what life is all about, and it doesn't matter. Explore the world. Nearly everything is really interesting if you go into it deeply enough."

Richard P. Feynman

TU DELFT

Abstract

3ME
Department of Precision and Microsystems Engineering

Master of Science in Mechanical Engineering

Influence of Mode-Coupling on Q-factor in Nanomechanical Resonators

by M.A. TEN WOLDE
4757769

Nanomechanical resonators with low dissipation rates are ideal tools in fundamental science applications. They have been used in the field of cavity optomechanics for example in ground-state cooling [1], [2], and in sensing applications, such as atomic resolution mass sensors [3], [4]. Their great sensitivity is due to their high Q-factor, which is a metric that shows how fast a system loses its energy [5]. In ultra-high Q nanomechanical resonators, energy loss is limited to intrinsic and radiation losses, the latter is due to energy dissipation from the resonator into the substrate [6]. Experiments have shown that the Q-factor of resonators with thin substrates are limited by radiation loss [7]. However, the precise role of the substrate remains a topic that has not received much attention, but has significant implications for how we design nanomechanical microchips. Here we show that the resonator mode can couple to nearby substrate modes, which reduces the Q-factor. We found that the strength of this mode-coupling depends on the mode-shape of the substrate, with stronger coupling at anti-nodes of the mode-shape and hardly any coupling at the nodes. Furthermore, we show that clamping down the substrate with double-sided tape reduces the Q-factor of the resonators, this is explained by a reduction in Q of substrate modes due to the tape. Lastly, we found that in thin substrates, which have a higher density of modes, the Q-factor can be limited due to mode-coupling with the substrate. Our results demonstrate that the substrate choice, as it can strongly affect the Q-factor of resonators, should become an integral part of the resonator design phase. These results can likely be used by all types of nanomechanical resonators limited by radiation loss. We can use this knowledge to design chips with resonators that have an even higher Q-factor.

Acknowledgements

I would like to thank Richard and Peter for the opportunity to do this project, and the introduction to the interesting field of nanomechanical resonators with this project, they taught me a lot about research in general as well. Their willingness to help and creative ways of thinking was a nice addition to our weekly meetings. In this project, I could almost daily discuss progression and problems with Matthijs, which I am very thankful for. His enthusiasm for guiding me in my research and always willing to answer my questions helped to deliver these results. In addition, I would like to thank the members of the Norte lab for our weekly meetings. Especially Andrea, Dongil, and Minxing for their feedback, input when solving problems, and fabrication of samples. The weekly discussions were fun and intriguing. I have learned a lot from your projects. Furthermore, I would like to thank my family and friends for showing interest in a project I was doing for over a year, for showing support, and for having great discussions. In particular, Wouter, Michiel, Bram, Thomas, Cedric, and Brian, with whom I talked the most. Lastly, special thanks to my girlfriend, Soleine. It was a difficult year, not only because of this project, but also because of Covid, and the loss of my mother. Most of our time was spent in an apartment a little too small for two people. I am grateful for your unending support, and your love for me.

Contents

Abstract iii

Acknowledgements v

1 Introduction 1
- 1.1 State of the art 1
- 1.2 Current research 2
- 1.3 Research objective 5

2 Theoretical background 7
- 2.1 Fundamentals of nanomechanical resonators 7
  - 2.1.1 Eigenfrequency analysis 7
  - 2.1.2 Frequency response 8
  - 2.1.3 Quality factor 9
  - 2.1.4 Loss mechanisms 11
  - 2.1.5 Fabrication process 12
- 2.2 Mode-coupling 13
  - 2.2.1 Two coupled bodies 14
  - 2.2.2 Hybridized Q-factor 14
  - 2.2.3 Frequency spacing 15
- 2.3 Conclusion 17

3 Methods 19
- 3.1 Numerical simulations 19
  - 3.1.1 String model 19
  - 3.1.2 Mode-shape dependence 20
  - 3.1.3 Film and substrate thickness 20
  - 3.1.4 Substrate damping 21
  - 3.1.5 Manipulating the resonance frequency 21
- 3.2 Measurement setup 22
- 3.3 Experimental measurements 23
  - 3.3.1 Substrate characterization 23
  - 3.3.2 Influence of clamping 23
  - 3.3.3 Influence of frequency spacing 24

4 Results and discussion 25
- 4.1 Mode-shape dependence 25
  - 4.1.1 Substrate characterization 25
  - 4.1.2 Nodes and anti-nodes 26
- 4.2 Mode-coupling 27
  - 4.2.1 Influence film thickness 27
  - 4.2.2 Influence substrate thickness 28
  - 4.2.3 Influence of substrate damping 29

4.3 Experimental: Chip clamping 30
  4.3.1 Influence of tape on Q-factor 30
  4.3.2 Analysis of the frequency response 30
  4.3.3 Clamping discussion 31
4.4 Experimental: frequency spacing 32
  4.4.1 Crossing a substrate mode 32
  4.4.2 Frequency spacing discussion 32

5 Conclusion and Outlook **35**
5.1 Conclusion 35
5.2 Recommendations and outlook 36

A Appendix **37**
A.1 Nominal values for trampoline resonator 37
A.2 Results of parameter sweep on resonance frequency 37
A.3 Sample in vacuum chamber 38
A.4 Substrate frequency comparison 38
A.5 Gas damping limited Q-factor 39
A.6 Mode-shape of the PhC chip 40
A.7 Q-factors of the PhC chip 41

Bibliography **43**

Dedicated to Friedel Filius,
may you rest in peace

1 Introduction

1.1 State of the art

In this thesis, we study very sensitive nanomechanical resonators. Resonators with very low dissipation rates make ideal tools for use in fundamental science applications. They have been used in the field of cavity optomechanics [8], for example in ground-state cooling [1], [2] and detecting single electron spin [9]. They have also been used in sensing applications, being able to sense masses with atomic resolution (sub-zeptogram) [3], [4] and sub-attonewton forces [10]. Their great sensitivity is due to their exceptionally high *quality factor*, which is a metric that states how fast a system's energy dissipates, or inversely, how well the resonator is isolated from its surrounding thermal environment.

An important step to increase the quality (Q) factor was shown in ref. [11], where they increased the stress of doubly clamped string resonators. This technique is now called dissipation dilution [12]–[14] and makes use of the fact that the added tension in the resonator is lossless while the overall energy increases, see equation 1.1. Currently, most of the very sensitive resonators at room temperature are made of thin high-stress silicon nitride (Si_3N_4, i.e. SiN) to reduce energy loss even further.

$$Q_{str} = 2\pi \frac{W_{tension} + W_{bending}}{\Delta W_{bending}} \tag{1.1}$$

The highest Q-factors were achieved using a so-called *soft clamped* approach [15]–[17], examples shown in fig. 1.1. These resonators make use of a repeating pattern that creates a phononic bandgap. With this technique, they are able to localize the mode in the center of the resonator, see inset of fig. 1.1b, and reduce bending at the clamping points and thus suppressing radiation loss. At room temperature, they achieve Q-factors >10^8, meaning

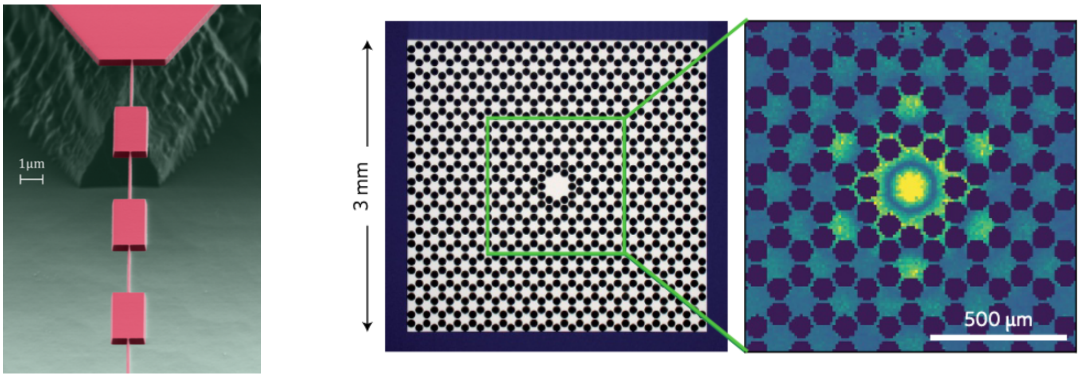

(A) Image adapted from [15]

(B) Image adapted from [16]

FIGURE 1.1: Examples of (A) 1D and (B) 2D phononic shields.

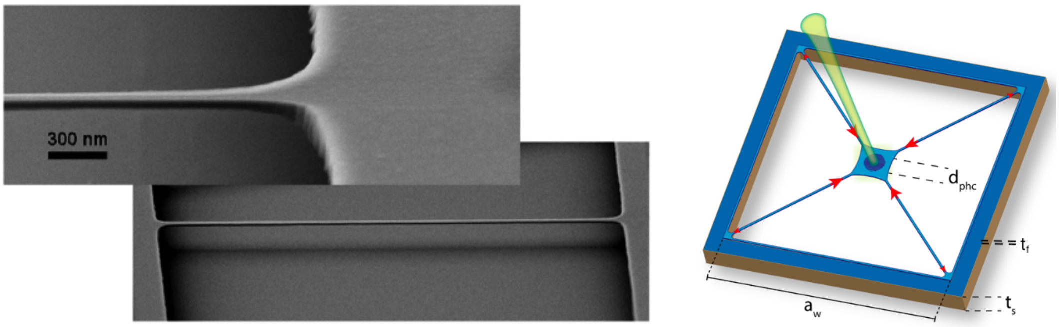

(A) Image adapted from [11]

(B) Image adapted from [7]

FIGURE 1.2: Examples of doubly clamped string resonator (A), and trampoline membrane resonator (B).

sensitivities limited by thermomechanical force noise at the aN/$\sqrt{\text{Hz}}$ level; and $f \times Q$ products of >10^{14} Hz, sufficient for quantum experiments at room temperature. However, they have several disadvantages due to the nature of the principle used to achieve 'soft clamps'. Firstly, they need a large number of repeating elements, making the system relatively large (length scale of several millimeters for MHz frequencies [15]–[17]), making chip-scale integration difficult. Secondly, the fragile structure can have difficulties with dissipation of heat accumulated from the detection laser, which is the main method of reading out the signal. Thirdly, soft clamping can only be applied to higher-order modes [18], while in practical sensing applications the fundamental mode is usually preferred because it has the lowest stiffness and cleanest spectral background. Lastly, these large and thin structures are often difficult to fabricate.

Alternative means of reaching these great sensitivities was shown using doubly clamped string [12], [19], membrane [20], and *trampoline* resonators [7], [21], of which the latter has achieved the highest Q-factors reaching 10^8, and $f \times Q$ products reaching 10^{13} Hz. These devices are also limited by thermomechanical force noise at the aN/$\sqrt{\text{Hz}}$ level and have sufficient $f \times Q$ products to enter the optomechanical quantum regime at room temperature [7], [20], [21]. Examples of these types of resonators are shown in fig. 1.2. Because these types of resonators do not suffer from the disadvantages associated with the soft clamped approach, they are easier to implement in real applications.

1.2 Current research

The highest Q-factors were achieved using the soft-clamped approach, being able to focus on minimizing the intrinsic loss. But, as mentioned before, this comes with several disadvantages for practical use. There is motivation to avoid complicated repeating patterns and to keep the length scales small. However, we also see a general trend that the Q-factor decreases with decreasing dimensions of the resonator ($Q \propto L/t$), attributed to losses at the resonator surface due to the increased surface-to-volume ratio [22]. The alternative 'trampoline' resonators showed ultra-high Q-factors (reaching 10^8 at 150 kHz, with a length scale of roughly 700 µm), without the disadvantages of the soft clamped approach. With these structures, it is not so clear which loss mechanism is limiting the Q-factor because it required a more in-depth look into the interaction of nanomechanical resonators and the substrates these resonators are fabricated on. While many experiments point to an important interplay between the resonators and the substrate [7], [12], [20], [23]–[26], to date, the exact mechanism of this coupling remains unknown.

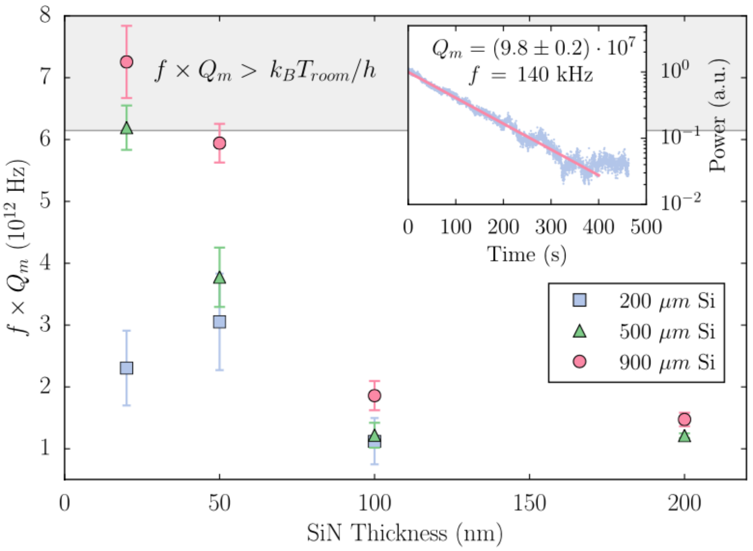

FIGURE 1.3: The effect of substrate and SiN thickness on the Q-factor in trampoline resonators. Adapted from [7].

Trampoline resonators can be considerd to be a combination of string and membrane resonators, for which significant research has been done. Studies say that for short string resonators radiation loss dominates, while for long strings (>100 µm) bending loss dominates [15]. For membrane resonators (L=0.5-5 mm) the radiation losses were limiting the Q-factor [20]. Another study found that in strings the high stress and increased string width increased coupling to the substrate and therefore radiation losses dominate, and for narrow low-stress strings, intrinsic material friction starts to limit the Q-factor [12]. The Q-factor for fundamental modes of long, thin doubly clamped nanostrings dominated by bending loss can be expressed as [12]

$$Q_{str} = \left[\frac{\pi^2 E}{12\sigma} \left(\frac{t_f}{L} \right)^2 + 1.0887 \sqrt{\frac{E}{\sigma}} \left(\frac{t_f}{L} \right) \right]^{-1} Q_{bending}, \tag{1.2}$$

where E is the Young's modulus of Si_3N_4, σ is the stress in the string, t_f is the film thickness, L is the length of the nanostring, and $Q_{bending}$ is the Q-factor due to bending losses in a relaxed string. If the resonator is dominated by bending loss we expect the Q-factor to increase when decreasing the SiN film thickness t_f. Furthermore, some enhancement in Q was found with 30-50 nm thick square membranes when moving from 200 to 500 µm thick substrates [27]. To test this on high-stress trampoline resonators, the SiN film thickness t_f and substrate thickness t_s (see 1.2b) were varied in ref. [7]. In figure 1.3 the $f \times Q$ products of trampoline resonators are shown. We assume that, within a given film thickness, the resonance frequency f does not vary, and thus we can consider the graph to show a scaled Q-factor.

From the graph, we see that with thick substrates (>500 µm) equation 1.2 holds and thus the Q-factor is limited by intrinsic loss, but for thin substrates (<200 µm) the radiation loss completely dominates (other loss mechanisms have been excluded, these will be explained further in section 2.1.4). This is an important observation because the substrate is hardly ever considered. The question remains, why is it only limiting thin substrates and not thicker substrates?

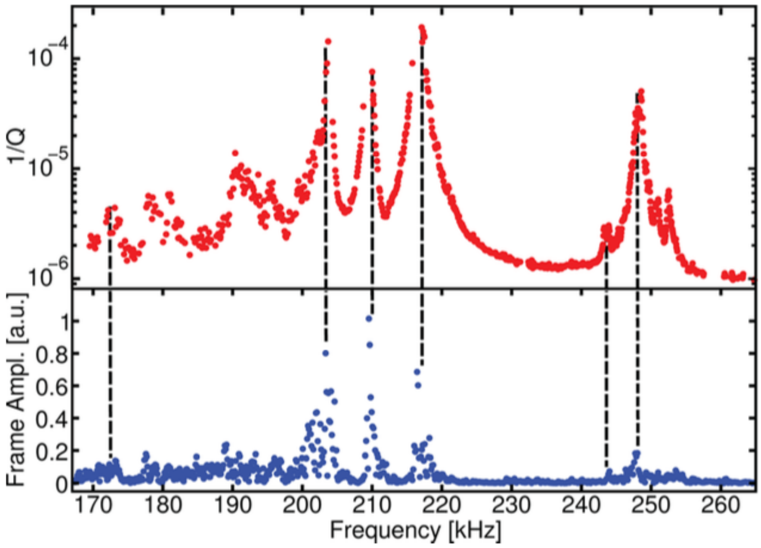

FIGURE 1.4: Spectrum of energy dissipation (top), and vibrations of the frame measured close to the membrane (bottom). Adapted from [26].

Radiation loss is the loss of mechanical energy arising from the coupling to the supporting substrate. Various treatments and models of radiation loss have been developed [23], [24], [28]. For simulations a perfectly matched layer (PML), which is a perfectly absorbing artificial boundary, is often used to compute radiation loss [15], [29], [30] using FEM software.

Currently, radiation loss is often studied in the context of 'phonon tunneling' [31], which sets up a quantum model for the motion experienced by each resonance of the suspended structure. The substrate is here considered as an elastic half-space, where the resonator phonons that leak out can propagate into (scattering states). With this technique, it was shown that anchor placement could limit the radiation loss in 'free-free' resonators [32], and that radiation loss was suppressed in higher harmonic modes using membrane resonators [20], [25]. Most studies investigate resonator design, but with radiation loss, the substrate is also important to investigate because it is the energy loss due to coupling with the substrate.

One would assume that with a thicker substrate, there would be less bending of the substrate; therefore less energy can propagate into the low Q substrate, and less energy is lost. There have only been a few studies on the influence of substrate thickness on Q-factor, in particular [23], [24], [30]. They conclude that with increasing substrate thickness, the Q-factor increases up to several orders of magnitude. Note that in these studies millimeter size resonators were experimentally compared. However, their theory would also be applicable for µm and nm size resonators. The reason is that normally in nano-scale devices other losses dominate, such as gas damping (which increases rapidly when the resonator's surface- to volume ratio increases [6]), but in ultra-high Q devices, this might not be the case.

Another important observation was an increase in energy dissipation of more than two orders of magnitude in membrane resonators due to coupling to modes of the frame [26], see fig. 1.4. However, a lot of questions remain, particularly when comparing the increase in dissipation to the relative frame amplitude. We notice that between 200 and 220 kHz the frame amplitude is relatively large (~0.8 of max amplitude) compared to that at 250 kHz (0.2 of max amplitude), while the energy dissipation is approximately equal ($1/Q = \sim 5 \times 10^{-5}$) in both points. How this can be explained has not yet been investigated.

Lastly, the resonator is attached to the substrate, but this substrate is also connected to something (e.g. piezo, or sample holder). Studies have shown that any type of clamping or gluing of the substrate to the experimental setup can reduce the Q-factor. The Q-factor of square membrane resonators drops from 4×10^6 to $<10^5$ when using glue as clamping [27], and a drop from 6×10^6 to 3×10^6 was observed in string resonators using tape as clamping [12]. Thus, radiation loss is increased by using any form of clamping, but the exact mechanism behind this is still unknown.

1.3 Research objective

From the current research, we can conclude that radiation loss remains an important loss mechanism, limiting the Q-factor in compact nanomechanical resonators. Most research is dedicated to investigating resonator geometry, while the substrate is also important to consider. Besides the thickness, the geometry of the substrate is generally ignored. To design ultra-high Q nanomechanical resonators we need to understand what is limiting the Q-factor. Understanding the resonator's mode-coupling to the substrate is crucial to this because energy dissipation can increase orders of magnitude when coupling to the substrate [26].

In this thesis, we want to investigate the influence of substrate modes on the Q-factor. Thus our research objective is *"understanding the influence of substrate mode-coupling on Q-factor in thin nanomechanical high-stress SiN resonators"*. Here we will shift our focus mostly on the substrate rather than the resonator, and importantly consider discrete eigenmodes of the substrate instead of a continuum of scattering states. The hypothesis is that the Q-factor can be limited due to mode-coupling with the substrate. Different aspects of the substrate will be analyzed.

First, in chapter 2 the reader will be introduced to the theoretical background information. Here we cover the basics of resonators, the Q-factor, different loss mechanisms, and the concept of mode-coupling. A simple 2 DOF analytical model is used to calculate the hybridized Q-factor of a resonator stacked on top of a heavy and relatively strongly damped substrate. As far as we know, this approach has not been presented in the literature.

Then, in chapter 3 the methods to numerically and experimentally test the hypothesis are presented. Here we look at numerical models with which we can test mode-coupling with a more complex geometry. We consider the mode-shape, substrate thickness, and damping of the substrate, and see how this changes the coupling behavior. Furthermore, we show the measurement setup and explain the different experiments that will be performed.

Next, in chapter 4 the results of the simulations and experiments are presented and discussed. Ring-down measurements are used to measure the Q-factor of fabricated resonators. Furthermore, the frequency response is analyzed and we spatially resolve the mode-shape of the substrate.

Lastly, this thesis finalizes with the conclusion and outlook for this study in chapter 5. Here we discuss the importance of the substrate. We have found that considering the substrate and designing the resonator optimally, implying minimized mode-coupling to the substrate, can improve the Q-factor of resonators limited by radiation loss.

2 Theoretical background

In this chapter, the theoretical basis of the topics in this thesis is described. We start with the fundamentals of the mechanical resonator in section 2.1. Then we present a simple analytical model for two coupled bodies in section 2.2, here we analyze the influence of mode-coupling on the Q-factor in a two-body system.

2.1 Fundamentals of nanomechanical resonators

A resonator is a system that oscillates with greater amplitude at certain *resonance* frequencies. Here we discuss a mechanical resonator, and thus the oscillations are mechanical excitations, i.e. *phonons*.

2.1.1 Eigenfrequency analysis

When we want to characterize the dynamics of a system we can look at the resonance frequencies and normal modes (or mode-shape). The resonance frequency is the frequency at which a system tends to oscillate in the absence of a force. When a system is vibrating at a certain resonance frequency, it deforms into a specific shape, the so-called normal mode. A normal mode is a sinusoidal motion of the system at a specific (resonance) frequency with a fixed phase relation. The motion of a system can be described by a superposition of the normal modes (from now on, *mode*). Let us look at a simple model of a 1 degree of freedom (DOF) resonator, see top right in figure 2.1, a mass-spring-damper system. The equation of motion (EOM) for the mass m_1 with spring constant k_1 and damping coefficient c_1 is

$$m_1\ddot{x}_1 + c_1(\dot{x}_1 - \dot{x}_0) + k_1(x_1 - x_0) = 0. \tag{2.1}$$

We divide the equation by m_1, and define $\omega_0 = \sqrt{k_1/m_1}$ and $\gamma = c_1/m_1$. In the absence of a force ($x_0 = 0$), it simplified to

$$\ddot{x}_1 + \gamma\dot{x}_1 + \omega_0^2 x_1 = 0. \tag{2.2}$$

Since we expect oscillatory motion we try

$$x_1(t) = \mathrm{Re}(X_1 e^{i\omega t}), \tag{2.3}$$

with amplitude of the motion X_1, frequency ω, and time t. Substituting 2.3 into 2.2 we get

$$-\omega^2 X_1 e^{i\omega t} + i\omega\gamma X_1 e^{i\omega t} + \omega_0^2 X_1 e^{i\omega t} = 0. \tag{2.4}$$

After simplifying and collecting terms we get

$$\left[(\omega_0^2 - \omega^2) + i\omega\gamma_1\right] X_1 = 0. \tag{2.5}$$

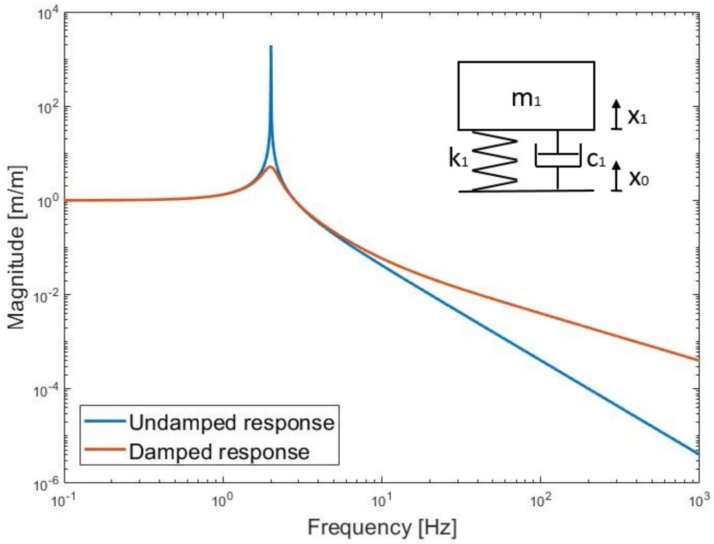

FIGURE 2.1: Frequency response of a 1 DOF mass spring damper system.

Here we have the classic eigenvalue problem (in non-matrix form), with a complex eigenvalue ω (resonance frequency) and eigenvector X_1 (mode-shape). Therefore, this analysis is also called the *eigenfrequency analysis*. Note that the amplitude of this motion can not be extracted from this analysis, only the direction it moves (defined by x_1 and x_0), which in this case is up and down motion (in multi-DOF we call this the mode-shape). When damping is very low, i.e. $c \ll \sqrt{mk}$, we can approximate the resonance frequency is ω_0, corrected by

$$\begin{aligned} w_r &= w_0\sqrt{1-2\zeta^2} \\ \zeta &= \frac{c_1}{2\sqrt{m_1 k_1}}. \end{aligned} \tag{2.6}$$

2.1.2 Frequency response

Now we want to analyze how the system responds to a vibration input by looking at the frequency response of the system. This is a measure of the magnitude and phase of the output of a system as a function of frequency, in comparison to the input. Let us look at the same 1 DOF example, see figure 2.1, with $m_1 = 1$, $k_1 = 158$, and $c_1 = 0$ and 1.25 for undamped and damped response respectively. Here the input is an oscillatory motion x_0 of the base ($x_0(t) = X_0 e^{i\omega t}$), thus we look at the transmissibility of the system. We start with the EOM

$$m_1\ddot{x}_1 + c_1\dot{x}_1 + k_1 x_1 = k_1 x_0 + c_1\dot{x}_0. \tag{2.7}$$

After substituting oscillatory motion, and collecting terms we get

$$\left[(\omega_0^2 - \omega^2) + i\omega\gamma\right] X_1 e^{i\omega t} = \left[\omega_0^2 + i\omega\gamma\right] X_0 e^{i\omega t}. \tag{2.8}$$

We divide output by input and calculate the frequency response $X(\omega)$ as

$$X(\omega) = \frac{X_1}{X_0} = \frac{\omega_0^2 + i\omega\gamma}{(\omega_0^2 - \omega^2) + i\omega\gamma}. \tag{2.9}$$

To get the frequency response, we plot $X(\omega)$, with magnitude $\|X(\omega)\|$ and phase $\phi(\omega) = \arctan\left(\frac{\operatorname{Im} X(\omega)}{\operatorname{Re} X(\omega)}\right)$, see figure 2.1. We see that the resonator follows the input 1:1 until there is a large increase in magnitude at 2 Hz, the resonance frequency ω_0. The more damping the system has, the lower this peak amplitude is, and the lower the Q-factor is. After the resonance, the magnitude starts to decrease (with a slope of 20 dB/decade).

2.1.3 Quality factor

The quality (Q) factor is a metric that states how fast a system loses energy [5], and is defined as

$$Q = 2\pi \frac{W}{\Delta W}, \tag{2.10}$$

With W the total energy stored in the system and ΔW being the energy lost per cycle. This means, that if the system loses relatively little energy, it has a high Q-factor. The great sensitivity of the resonators mentioned in section 1.1 is because of their exceptionally high Q-factor. The Q-factor is an important parameter in the context of sensors because it is inversely proportional to the thermomechanical force noise S_{FF} [16], [21], [33], which can be written as

$$S_{FF} = 2m_{eff}\frac{2\pi f}{Q}k_bT, \tag{2.11}$$

with the effective mass of the resonator m_{eff}, the resonance frequency f, the Boltzmann constant k_b, and temperature T. To give an intuitive sense of why a high Q-factor decreases the noise of a resonator, we think of what happens when a resonator is very well isolated from its (noisy) environment. If the system is very well isolated from its environment, not much energy is lost out of the system; this also means that not much energy, or noise, can enter the system. Isolation from outside noise is also of great importance to quantum technologies, which are extremely sensitive to outside environmental noise. This noise gets worse at room temperature.

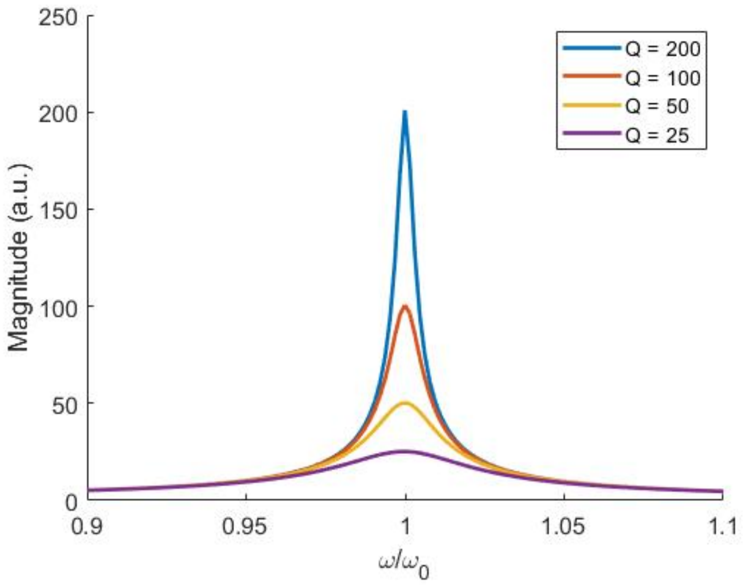

FIGURE 2.2: Frequency response of a 1 DOF resonator for different Q-factors.

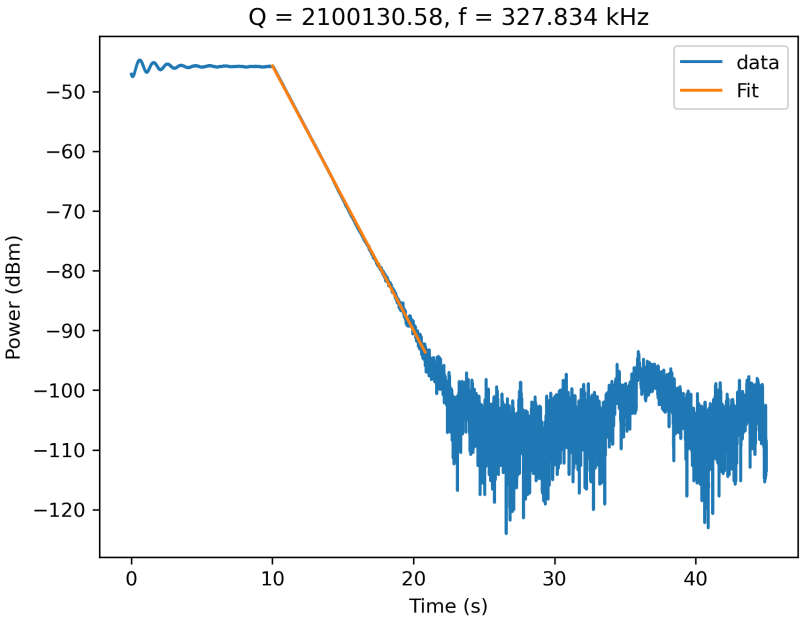

FIGURE 2.3: Example of a ring-down measurement performed on one of our experimental samples.

In figure 2.2 the frequency response of a 1 DOF resonator is plotted for different energy losses, with more energy loss meaning a lower Q-factor. When the Q-factor decreases, we see a reduction in peak amplitude, and the bandwidth of the mode gets wider (making it hard to determine which frequency the mode is exactly, which is useful for measurements). To determine the Q-factor of a system, multiple approaches can be taken. When the energy terms are known, equation 2.10 can be used. When the system becomes more complex this is not always a viable approach, since there might not be a known analytical solution for the EOM. In this case, we can extract the Q-factor from the complex-valued eigenfrequency ω_0 of the system [34], using

$$Q = \frac{\mathrm{Re}(\omega_0)}{2\,\mathrm{Im}(\omega_0)}. \tag{2.12}$$

This value can be determined either analytically or, in the case of more complex geometry, numerically. In real samples, the Q-factor can be measured in two ways. Firstly, equation 2.13 is used to determine the Q-factor. Here, $\Delta\omega$ is the full width at half maximum of the resonance frequency ω peak in the frequency response. In figure 2.2 the higher Q-factors have a more narrow bandwidth. When the width gets too thin, the second method is used, namely a ring-down measurement. Here, the resonator is driven on resonance until a steady-state amplitude, then the input is stopped and the amplitude is measured over time and it 'rings down'. The data is fitted to an exponential function, which allows for the calculation of the Q-factor [35], see fig. 2.3 for an example of a ring-down fit.

$$Q = \frac{\omega_r}{\Delta\omega}. \tag{2.13}$$

There is a well-known trade-off between the Q-factor and resonance frequency (f). When increasing Q, most of the time f decreases. For opto-mechanical quantum experiments, the $f \times Q$ product is a parameter, which plays an important role in the phase noise performance of oscillators [8]. It quantifies the decoupling of the mechanical resonator from a thermal environment. Specifically,

$$\frac{\Omega_m}{\bar{n}_{\mathrm{th}}\Gamma_m} = Q_m f_m \times \left(\frac{h}{k_B T}\right) \tag{2.14}$$

denotes the number of coherent oscillations ($\bar{n}_{\mathrm{th}}$) in the presence of thermal decoherence and evidently scales with $f \times Q$ [8]. With the frequency Ω_m, the damping rate Γ_m, Planck's constant h, Boltzmann constant k_B, and the temperature of the environment T. It denotes the number of oscillations the resonator makes as a quantum object before one phonon of environmental noise enters the system and destroys its coherent quantum nature.

2.1.4 Loss mechanisms

The Q-factor depends on the energy lost per cycle, as seen in section 2.1.3. A system can lose its energy through different loss mechanisms. Here we discuss the most important loss mechanisms for nanomechanical resonators. These loss mechanisms have extensively been investigated and reviewed [6], [8], [36], [37]. There are different conventions used in regards to naming the loss mechanisms, it is therefore important to clarify how we interpret them. We divide the loss mechanisms into three groups: 1) viscous damping, 2) intrinsic dissipation mechanisms, and 3) radiation losses.

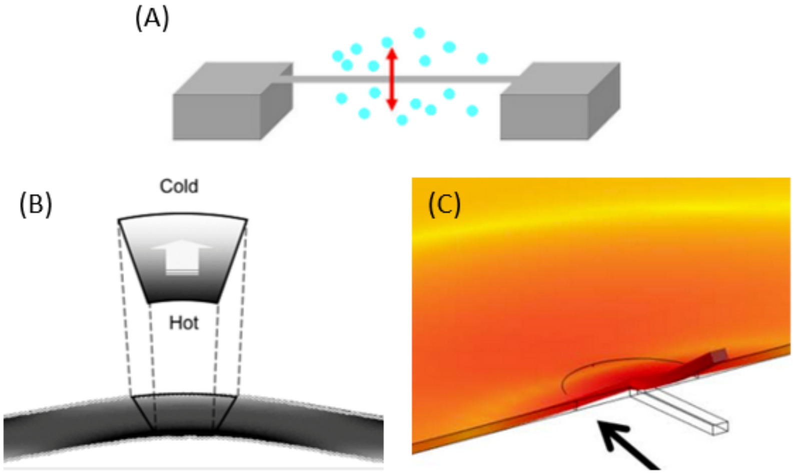

FIGURE 2.4: Examples of the three groups of loss mechanisms. A) gas damping, adapted from [38] B) intrinsic loss mechanism (TED), adapted from [39], and 3) radiation loss where we can see the elastic waves propagate into the substrate, adapted from [30].

- *Viscous damping*, which is caused by interactions with the surrounding gas atoms or by compression of thin fluidic layers. Air damping increases rapidly as the resonator's surface- to volume ratio increases [6], and is, therefore, important in nanomechanical resonators. Viscous damping depends on pressure and can be divided into three regions [6], [40]: viscous, molecular, and intrinsic region. Where in the latter region air pressure is so low, it becomes negligible.

- *Intrinsic losses*, where we consider: 1) *bending loss*, or material loss, which is caused by the relaxation of defect states in the bulk or surface of the resonator. These losses are described by a complex-valued Young's-modulus $\tilde{E} = (1 + i\eta)E$, where η is defined as the intrinsic loss factor [41]. And 2) *thermoelastic dissipation* (TED) which is mechanical loss due to heat conduction. It is attributed to an oscillating transversal heat flow in the beam. During vibration, one side of the beam is under compression while the other is under tension. Stress induces a change of temperature in the beam, with tension producing temperature decrease and compression producing temperature increase [6].
- *Radiation loss*, or clamping/anchor/acoustic loss, is energy dissipation due to the radiation of elastic waves into the substrate through the supports of the resonator. The behavior of the resonator is affected by the boundary conditions, i.e. the substrate or the clamping. The substrate is not infinitely rigid, therefore some of the energy is lost into the substrate. Radiation losses can be modeled with a perfectly matched layer (PML) [15], [36], which absorbs incoming waves from all angles without reflections.

$$\frac{1}{Q_{total}} = \frac{1}{Q_{viscous}} + \frac{1}{Q_{bending}} + \frac{1}{Q_{TED}} + \frac{1}{Q_{radiation}} \tag{2.15}$$

Loss mechanisms contribute independently to the total Q-factor. From equation 2.15, we can conclude that not all loss mechanisms are as important, with some being more dominant and some being negligible (in literature sometimes energy dissipation $\frac{1}{Q}$ is given instead of Q). For example, if $Q_{viscous}$ would be 10, and all others 10^9, then the resulting Q_{total} would be 10, thus being completely dominated by the viscous damping. In this research we are focusing on resonators with certain criteria such that the following applies: 1) In the case that the resonator is put in a sufficiently high vacuum, the viscous damping starts to be negligible [6], [19]. This can easily be tested by measuring the Q-factor while decreasing the pressure. When further decreasing the pressure does not influence the Q-factor anymore, we can assume that the viscous damping is negligible at that point. 2) Thermoelastic dissipation can be analytically calculated. By using thin high-stress SiN resonators, the thermoelastic loss is negligible [27], [42]–[44]. That leaves bending and radiation loss. Radiation loss can be limited by using a phononic shield, as in the soft-clamped designs, but this came with several disadvantages, see section 1.1.

Regarding the resonators we use in this thesis, it is important to investigate which loss mechanism(s) is (are) dominating. The reason is that in this project we study mode-coupling with the substrate, which is part of radiation loss. If another loss mechanism is much higher, e.g. limited by gas damping due to high pressure, we cannot see the effect of mode-coupling.

2.1.5 Fabrication process

Nanomechanical resonators are fabricated in different ways (e.g. [15], [16], [21]). Here the fabrication process of the trampoline resonator used in the experiments is presented, example shown in fig. 2.6. We start with a Si ⟨100⟩ wafer with a thickness of ranging from 200 µm-1 mm on which a layer of 50-100 nm SiN is deposited with low pressure chemical vapor deposition (LPCVD) at a temperature of 800 °C (fig. 2.5a). Due to the difference in the coefficient of thermal expansion, as the chips cool down, the SiN contacts more than Si, resulting in a net tensile stress (~1 GPa) of the SiN film at room temperature. Then, a positive electron beam resist (ARP6200) is spun on the chip (fig. 2.5b). This layer is patterned using a Raith electron beam pattern generation (EBPG) 5200 lithography system. The pattern is an array of 3x3 or 5x5 trampoline resonators on a single chip, with this we can sweep parameters to change the behavior of the resonators, but keep the substrate the same. The

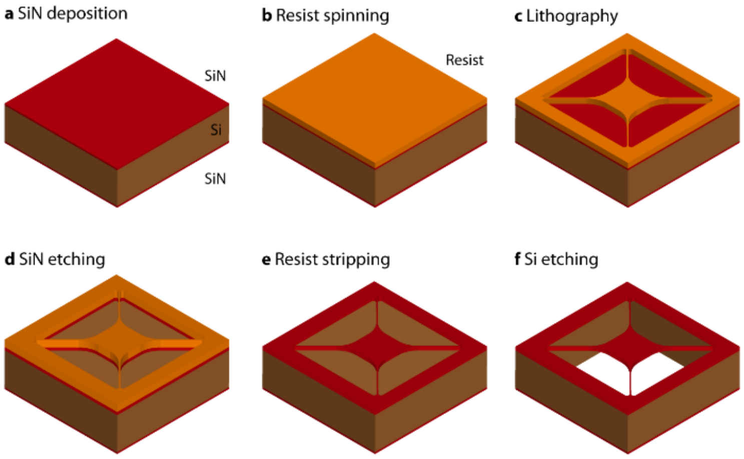

FIGURE 2.5: Fabrication process for the nanomechanical resonators used in this thesis, image adapted from [45].

resist, exposed to the electron beam, is developed using pentyl acetate (fig. 2.5c). Next, the pattern is etched in the SiN using reactive ion etch (ICP-RIE pseudo-Bosch) with a plasma of CHF_3 at 20 °C (fig. 2.5d). The electron beam resist is removed and the chip is cleaned with an O_2 plasma and a piranha (H_2SO_4/H_2O_2) solution before being dipped in hydrofluoric acid to remove any oxidation (fig. 2.5e). Lastly, the SiN layer needs to be released from the Si substrate, which is done with a fluorine-based dry release (fig. 2.5f). This step does not require a mask given the high selectivity of the chosen chemical against SiN, avoiding any additional cleaning step.

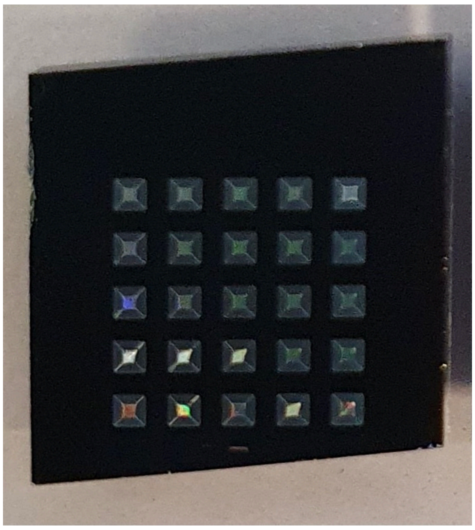

FIGURE 2.6: Example of one of the resulting chips (10 mm × 10 mm) with 25 trampoline resonators.

2.2 Mode-coupling

One way to understand energy loss is to see how much energy dissipates from the resonator into the substrate due to them being coupled (radiation loss). Until now we considered the resonator to be connected to an infinitely stiff and heavy base. However, in reality, the resonator is fabricated on a substrate with finite mass and stiffness. It, therefore, has resonance frequencies, with mode-shapes, and losses. These two bodies are coupled to each other. Due to coupling, the modes of these bodies *hybridize*, and some energy radiates into the substrate. Now assume the resonator has a relatively high Q mode, and the substrate a low Q mode. The leaked energy is lost more quickly in the substrate because of the higher damping (low Q-factor). In this section, we create an intuitive analytical model to investigate what happens when a high Q resonator mode couples to a low Q substrate mode. This interaction and energy exchange between the two modes is called *mode-coupling*.

2.2.1 Two coupled bodies

First, let us set up an analytical model to study the physics. We have a simplified and theoretical substrate and resonators with masses $m_1 = 1 \times 10^{-4}\,\mathrm{kg}$ and $m_2 = 5 \times 10^{-11}\,\mathrm{kg}$, respectively (which is a reasonable mass ratio for substrate and nanomechanical resonators). The resonator has a spring constant $k_2 = 177.65\,\mathrm{N\,m^{-1}}$ and damping coefficient $c_2 = 9.4 \times 10^{-13}\,\mathrm{N\,s\,m^{-1}}$, and is stacked on top of the substrate.

We compare two substrates: Firstly, a weakly coupled substrate where there is little energy exchange and interaction between the two modes, with spring constant $k_1 = 4.8 \times 10^7\,\mathrm{N\,m^{-1}}$ and damping coefficient $c_1 = 0.7\,\mathrm{N\,s\,m^{-1}}$. Secondly, a strongly coupled substrate, where there is interaction and energy exchange between the two modes, with $k_1 = 3 \times 10^8\,\mathrm{N\,m^{-1}}$ and damping coefficient $c_1 = 1.73\,\mathrm{N\,s\,m^{-1}}$. The aforementioned values result in a resonance frequency at $\sim 110 \times 10^3$ and 275×10^3 Hz for the weakly and strongly coupled substrates respectively, and to realize a large difference in Q-factor between resonator and substrate mode. The resonator and substrate coupled to each other, thus the EOM of the two bodies are

$$\begin{bmatrix} (k_1 - \omega^2 m_1) + i\omega c_1 & -\omega^2 m_2 \\ -(k_2 + i\omega c_2) & (k_2 - \omega^2 m_2) + i\omega c_2 \end{bmatrix} \begin{bmatrix} X_1 \\ X_2 \end{bmatrix} = \begin{bmatrix} (k_1 + i\omega c_1) \\ 0 \end{bmatrix} X_0. \tag{2.16}$$

First, we can look at the driven case (steady-state). To get the frequency response we calculate $\left|\frac{X_1}{X_0}\right|$, and $\left|\frac{X_2}{X_0}\right|$ as a function of frequency ω. The 2 DOF responses of the resonator coupled to the two substrates are plotted in fig. 2.7. We can identify the substrate mode in the frequency response of the resonator. A 2 DOF system, as seen from the figure, has two modes (in this case 1 substrate and 1 resonator mode). These two modes do not necessarily have the same Q-factor. Now we want to investigate how the substrate mode influences the resonator mode.

2.2.2 Hybridized Q-factor

Due to the low Q-factor of the substrate, its resonance peak is relatively wide compared to the very sharp peak of the resonator mode ($Q = \omega_r/\Delta\omega$), as can be seen in figure 2.7. We want to investigate the influence of mode-coupling on the Q-factor. Let us first determine the uncoupled Q-factor of the resonator, using equation 2.10. The total stored energy W can be calculated using $W = \max(\frac{1}{2}m_2\dot{x_2}^2)$, with $x = \mathrm{Re}(X_2 e^{i\omega t})$. Solving the equation results in $W = \frac{1}{2}m_2 X_2^2\omega^2$. As for energy lost per cycle, we have the dissipation term c_2, giving us the equation $\Delta W = \int_0^{2\pi/\omega_0} c_2\dot{x}_2^2 dt = \pi c_2 X_2^2 \omega$. Thus the expected (uncoupled) Q-factor can be calculated using $Q = 2\pi\frac{W}{\Delta W} = \frac{m_2\omega}{c_2} = \frac{\sqrt{m_2 k_2}}{c_2}$. In this case, with the values of the example above, the expected (uncoupled) Q-factor is $Q_2 = 1 \times 10^8$.

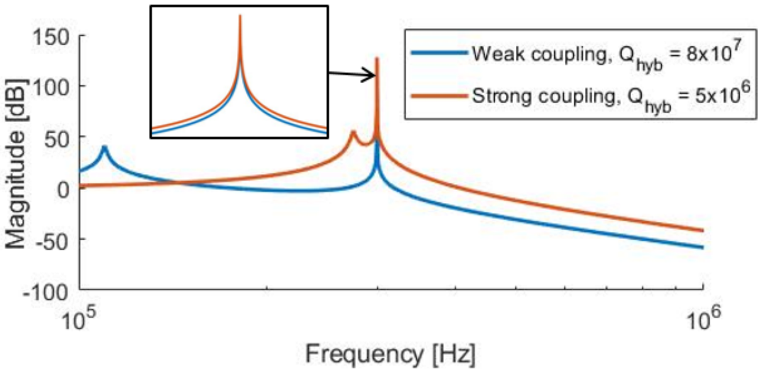

FIGURE 2.7: Frequency response of resonator (x_2) in a 2 DOF system, displacement amplitude [dB] vs frequency. In the weakly coupled response, the substrate and resonator do not exchange much energy, while in the strongly coupled response they do. This can be observed by the fact that the Q-factor is decreased. Inset: zoom-in of the resonance peak, the width of the peak is wider in the strongly coupled case.

Now we can look at the effective Q-factor for the coupled system, because they are coupled the two modes exchange energy and thus the Q-factor is hybridized. In section 2.1.3 we presented methods to determine the Q-factor of a system. Here we use equation 2.12, thus we need to calculate the eigenfrequencies ω_n of the system. We start with the EOM of the system using equation 2.16, but in the undriven case

$$\begin{bmatrix} (k_1 - \omega^2 m_1) + i\omega c_1 & -m_2\omega^2 \\ -(k_2 + i\omega c_2) & (k_2 - \omega^2 m_2) + i\omega c_2 \end{bmatrix} \begin{bmatrix} X_1 \\ X_2 \end{bmatrix} = \bar{\mathrm{F}}\mathbf{X} = 0. \tag{2.17}$$

For the non-trivial solution, we need to solve for which eigenfrequencies ω_n $\det(\bar{\mathrm{F}}) = 0$. We can use a numerical tool, like Matlab, to find the complex-valued roots ω_n of this 4th order complex polynomial. For the solution we only look at positive real roots, then we calculate the Q-factor use equation 2.12. When doing the calculations for the values from the example above, we get hybridized Q-factor of $Q_2^{hyb} = 8 \times 10^7$ in the weakly coupled case, we see that the coupling is weak because the Q-factor only drops from 1×10^8 to 8×10^7. When calculating the Q-factor of the strongly coupled case we get $Q_2^{hyb} = 5 \times 10^6$. They are strongly coupled because the Q-factor has a reduction of more than an order of magnitude, thus more energy is lost into the substrate per cycle. We can also see this visually because the width of the resonance peak is wider, see inset of fig. 2.7.

Thus, we see that the Q-factor of the resonator decreased from 8×10^7 to 5×10^6 when a substrate mode is nearby (note that the theoretical uncoupled Q-factor is even higher reaching 1×10^8). This decrease in Q-factor is caused by the fact that it is coupled to a low-Qsubstrate, i.e. energy dissipates in the substrate.

2.2.3 Frequency spacing

In the previous section, we calculated the hybridized Q-factor of a resonator with two different substrates, of which one had a substrate mode nearby. The Q-factor dropped with more than 1 order of magnitude when the substrate mode was closer to the resonator mode. Here we evaluate the hybridized Q-factors as a function of the frequency spacing ω_2/ω_1, where

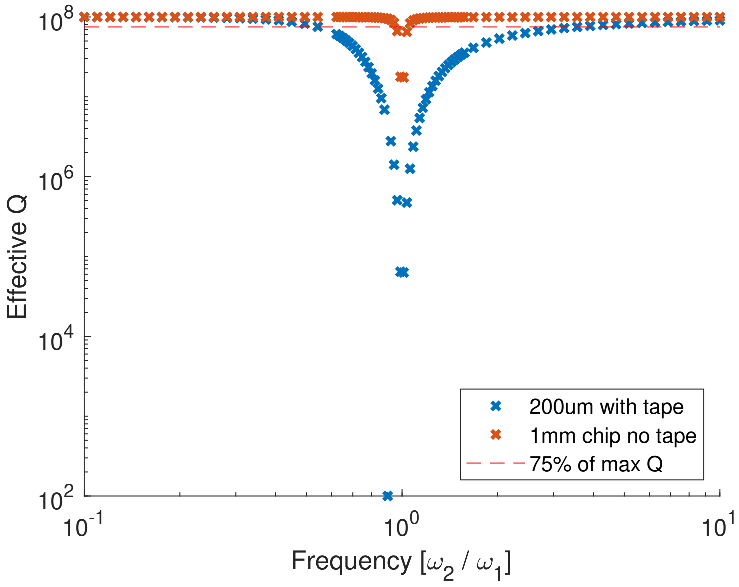

FIGURE 2.8: Comparison of the analytical solutions of the hybridized Q-factor of a light and relatively highly damped substrate (blue) with a heavy and less damped substrate (orange). Every cross is a solution for a resonator with different resonance frequency (10 kHz to 1 MHz).

ω_1 and ω_2 are the resonance frequency of the substrate, and resonator respectively. The resonance frequencies can be changed by adding or subtracting some mass or by changing the stiffness.

Studies found that the Q-factor of the resonator decreases with decreasing substrate thickness (in the radiation loss dominated regime) [7], [23], [24], [30], see section 1.2. The effect of decreasing the thickness t of the substrate is threefold: First, it decreases the mass, since $m \propto t$, to investigate this effect we also compare different masses m_1 in the analysis. Secondly, it decreases the stiffness, since $k \propto t^3$. Thirdly, it changes the resonance frequencies, since $\omega \propto \sqrt{\frac{k}{m}}$, thus $\omega \propto t$. This means there are twice as many modes when the thickness of the substrate is halved.

Furthermore, when taping a substrate down, the vibrational energy gets dissipated into the tape. Studies found that taping (or gluing) the substrate decreased the Q-factor of resonators [12], [27]. Therefore we compare different energy dissipation c_1 in the substrate.

Here we use mass $m_1 = 5 \times 10^{-5}$ kg and 2×10^{-4} kg which is roughly the mass of a Si $10 \times 10\text{mm}^2$ substrate of 200 µm and 1 mm thick respectively, and $m_2 = 5 \times 10^{-11}$ kg, which is roughly the mass of a suspended SiN trampoline resonator. For the substrate losses c_1 we define an uncoupled Q-factor of $Q_1 = 10^2$ and 10^4, which are reasonable values for substrate modes in different clamping conditions (i.e. taping the sample down or resting freely). Then we calculate the loss as $c_1 = \frac{\sqrt{m_1 k_1}}{Q_1}$ (see section 2.2.2). For the resonator loss c_2 we also define an uncoupled Q-factor of $Q_1 = 10^8$ (this would be its intrinsic limit), and calculate the loss the same way as c_1. The substrate mode is located at $\omega_1 = 100$ kHz, by using the relation $\omega_1 = \sqrt{k_1/m_1}$.

From the analysis we find 1) that the hybridized Q-factor of the resonator drops dramatically when the resonances overlap, and importantly 2) that the *'region of influence'* is larger when the substrate has a lower mass, and/or the substrate mode has a lower Q-factor. We have plotted the extremes in fig. 2.8. The shape of the graph is very similar to that observed by [26], see figure 1.4 (note that the inverse, $1/Q$ i.e. dissipation, is plotted). We see that with a thick substrate with low damping, the Q-factor is almost constantly at its intrinsic limit. However, with a thin highly damped substrate, the hybridized Q-factor is decreased significantly over a large region. For example, a resonator mode at $\omega_2 = 350\,\text{kHz}$ drops to $\sim 7.5 \times 10^7$. This means that the resonator mode 250 kHz removed from the substrate mode (at 100 kHz), can drop by more than 25 %. If the resonator mode is even closer, this effect is even stronger. This is an important observation because in this model there is only 1 substrate mode that can affect the resonator, while a real substrate has more modes which can deteriorate the Q-factor.

2.3 Conclusion

To conclude, resonant frequencies of mechanical resonators can be determined by either calculating the eigenfrequencies or from the peaks in the frequency response, each with a specific mode-shape. In a damped system, the magnitude at a mode is lower with higher damping, which means that that mode loses more energy. Minimizing energy loss increases the Q-factor, which in turn decreases the thermomechanical force noise of a resonator used as a sensor. Resonators made of thin high-stress SiN that are placed in high vacuum, are dominated by bending and radiation loss. The fundamental (geometric and material) limit is bending loss, but in some cases, radiation loss is dominating. Limiting mode-coupling with the substrate is one method of reducing radiation losses, and getting closer to the fundamental limit.

Mode-coupling is the interaction (energy exchange) between modes of a system. In this chapter, we assumed that a 1 DOF resonator is placed on a 1 DOF substrate, and analyzed the influence of mode-coupling on the Q-factor. Although this two mass-spring-damper model has been widely considered in many mechanics text-books, this is used for the first time to calculate the effects on the Q-factor in hybridized systems, and also relates it to behavior of (nano)mechanical resonators on a microchip.

We have found that mode-coupling can decrease the Q-factor significantly. In this simplified analytical model the Q-factor could decrease up to 25%, even when the mode of the resonator is 250 kHz removed from the substrate mode located at 100 kHz. When the resonator mode is even closer, it can even decrease up to several orders of magnitude. We can reduce the 'region of influence' of this mode-coupling by increasing the mass of the substrate or by decreasing the damping of the substrate. In this analytical model, there is only 1 substrate mode. To investigate the effect of multiple substrate modes we use numerical models, see section 3.1, where we can analyze more complex geometry.

3 Methods

In the previous chapter, we introduced a simple mathematical model of a resonator coupled to a substrate. However, that model is, of course, overly simplified. The 2 DOF model used in section 2.2 only has two modes while a real system has infinitely many. We want to affirm this mode-coupling effect both numerically and experimentally. In this chapter, we introduce the finite element method (FEM) to simulate resonator models with complex geometry, and the measurement setup with the experiments.

3.1 Numerical simulations

The simulations are done in COMSOL multiphysics. We use a variety of different models because for some simulations we want to sweep a multitude of parameter combinations, which, in the case of a very high fidelity model, can easily take a day of run time. This is of course not always practical and necessary. We, therefore, design models that are able to produce results for the specific case.

3.1.1 String model

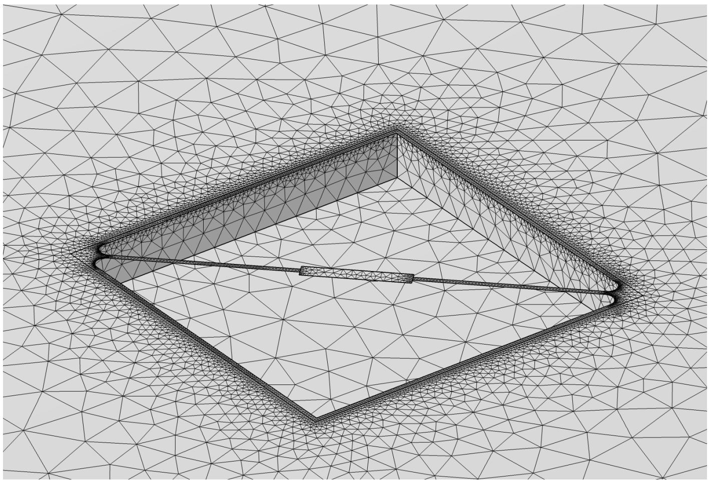

FIGURE 3.1: String resonator model with isotropic loss factor $\eta_s = 1 \times 10^{-3}$ in the substrate and $\eta_s = 1 \times 10^{-10}$ in the SiN resonator.

We start with a string resonator with nominal parameters as presented in table 3.1, of which we know that radiation losses are the dominating damping mechanism [12]. The model consists of a 3D structure of silicon, which acts as the substrate, and a 2D shell structure of SiN which includes the resonator (the resonator has a large aspect ratio typically >100 µm in length and <200 nm in thickness [7], [12], [21]). These two parts are connected using a thin-solid structure connection. An *'isotropic loss factor'* η_s is added to the material, this simulates the intrinsic loss of resonator (see section 2.1.4). With $\eta_s = 1 \times 10^{-3}$ in the substrate and $\eta_s = 1 \times 10^{-10}$ in the SiN resonator. We use this parameter as a fit parameter to achieve

Parameter	value
Si chip thickness	500 µm
SiN film thickness	50 nm
String width	10 µm
Fillet radius	20 µm
Initial stress	1 GPa
Overhang size	10 µm
Resonator length	700 µm
Substrate width	10 mm × 10 mm

TABLE 3.1: Nominal values for string resonator design parameter.

a large difference in the Q-factor between the resonator and substrate. The 2D SiN shell is under high initial tensile stress of 1 GPa, therefore we first simulate the static equilibrium (stationary study). This step computes the stresses and strains in the model and deforms the model accordingly. Afterward, the eigenfrequency analysis is performed, used to compute the eigenmodes and eigenfrequencies. Here we are able to plot the mode shape of the resonator and calculate the corresponding Q-factor at the computed eigenfrequencies.

3.1.2 Mode-shape dependence

In the analytical model both degrees of freedom, and thus motion, were in the same direction (x_1 and x_2). If one DOF was orthogonal to the other, it would imply that they would be uncoupled, that is, the motion of body 2 would not be affected by the motion of body 1 because the motion amplitude would not be in that direction. In numerical simulations, we consider in the order of 10^5 DOF. The result is distinct mode-shapes at the resonance frequencies. If we consider the two bodies to be the resonator and the substrate, some of the substrate-modes will have a large motion amplitude at the location of the resonator, while others do not. We suspect that resonator modes only couple to substrate modes where there is motion amplitude (in the same direction) in these modes.

Here we test this hypothesis by changing the location of the resonator such that it lies on a node / anti-node of a substrate mode and analyze if and how the location influences the mode-coupling. First, we model a 10x10 mm^2 by 500 µm thick silicon substrate with a 100 nm thin high-stress SiN film. We do not model the resonator, since that will not change the eigenfrequencies of the substrate significantly and reduces computation time. We use this to get an idea of the substrate mode-shape and compare it to experimental data to see if we can accurately predict the location of the substrate modes, and their shape. Then, to check the hypothesis, we use the string resonator model and simulate the resonator in two locations. The mass density of the center pad of the resonator is changed by multiplying the density of the material with a parameter. This is done to change the mass of the resonator and thereby changing the resonance frequency, as done in the analytical study, see section 2.2.3. By sweeping this parameter we can numerically verify the analytical results. We compare the calculated Q-factors of the node design with those of the anti-node location.

3.1.3 Film and substrate thickness

The results found in ref. [7] showed that in thin substrates the Q-factor is limited by radiation loss, see figure 1.3. Here we want to investigate the idea of mode-coupling in the context of that study. We do this by varying the film and substrate thickness of the string model w.r.t. nominal values, then sweep the mass of the center pad of the string (changing its resonance frequency) and thereby crossing different substrate modes.

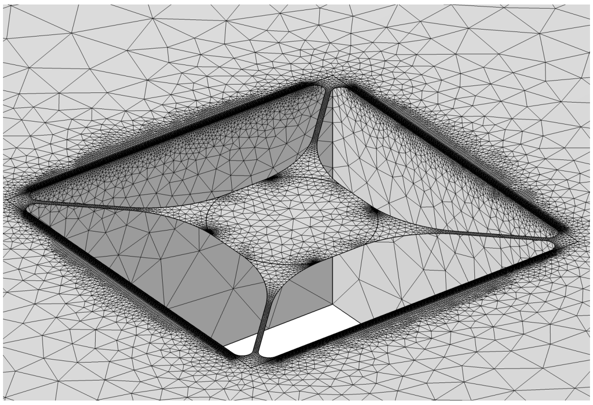

FIGURE 3.2: Trampoline resonator model created by [46]. It is used to determine a parameter to sweep the resonance frequency, and to design the chips for the experimental phase.

From equation 1.2, we expect the Q-factor to increase with thinner SiN films. We simulate for different film thicknesses (t_f), and plot the calculated Q-factor for each eigenfrequency of the resonator (different masses) and substrates. The goal is to 1) verify if decreasing the film thickness increases the Q-factor in this numerical model as the theory suggests, and 2) investigate if the film thickness has an influence on mode-coupling.

Next, it could be argued that with thinner substrates there is more bending of the substrate, and therefore more radiation loss. From our analytical models, it can be seen that thinner (lower mass) substrates, the 'region of influence' is larger. Furthermore, because thinner substrates are less stiff, the frequency spacing between modes is lower, that is, there is a higher density of modes. The aforementioned reasons could explain why resonators on thin substrates are dominated by radiation loss. We repeat the previous simulations, but now for different substrate thicknesses. The goal is to 1) verify if thinner substrates have a larger region of influence of mode-coupling, and 2) if mode-coupling can be limiting the Q-factor.

3.1.4 Substrate damping

When two modes couple, the Q-factor of the higher Q mode decreases, and that of the lower Q mode very slightly increases (heavily favoring the supporting body, see fig. 2.8). Previous studies showed that any form of clamping reduces the Q-factor of high Q resonators [12], [27]. Here we want to investigate if this can be explained due to mode-coupling. The idea is that if tape were to be used as a clamping method, as done in ref. [12], the added damping of the tape could reduce the Q-factors of substrate modes.

For this simulation, we compute the Q-factor of the string resonator, similar to the previous section, and compare differently damped (η_s) substrates. The expected result is that when a resonator mode couples to a relatively low Q substrate mode, the reduction in the Q-factor is higher, compared to when the resonator mode couples to a relatively high Q substrate mode.

3.1.5 Manipulating the resonance frequency

To experimentally see the influence of mode-coupling on the Q-factor, we want to apply the same technique used in the numerical simulations, i.e. changing the resonance frequency spacing between a substrate mode and resonator mode. Since a substrate parameter can not be changed in one sample (we compare Q-factors within one chip, to limit the variance due to fabrication), we look at the resonator design parameters. We want to control the resonance frequency of the resonator, without changing the overall behavior too much.

We model a trampoline resonator (see fig. 3.2), as used in the experiments. Again, it is a 2D SiN shell structure (incl. trampoline resonator) on top of a 3D Si substrate. No loss mechanism is added, because 1) the exact values are still unknown, 2) to limit computation time, and 3) it does not change the resonance frequencies significantly. A custom mesh setting is used to achieve a high fidelity at the small length-scale resonator while keeping the total number of nodes limited. The SiN film is under a high initial of 1 GPa, thus we first simulate the static equilibrium and then compute the eigenfrequencies. We decided to sweep the outer fillet, membrane size, tether width, and PhC ratio (=how much of the membrane is used as a photonic crystal, i.e holes) w.r.t. nominal values, see table A.1 in the appendix. Varying these parameters would be easy to fabricate in one chip.

The results are shown in appendix A.2. The first three parameters have also been measured in ref. [7], and received similar results with a slightly different design. The outer fillet also seems like a good parameter, but there is some debate about the influence of outer fillet on radiation loss [18], [47], and we want to carefully control what is happening. The same argument can be made for the tether width, since the tether width is closely linked to radiation loss, as $Q_{clamp} \propto \frac{L}{w}$ [7], [12]. Therefore those two were not chosen. Increasing the membrane size increases the amount of material that bends, creating more bending losses. Furthermore, the $f \times Q$ product changes, as found by [7]. As said before we want the minimum change in design because we only want to change the resonance frequency. Therefore, we chose to use the PhC ratio because it is easy to control (small increments), and it does not affect the other important parameters as much.

3.2 Measurement setup

In order to experimentally determine the influence of mode-coupling on the Q-factor, we use the setup outlined in fig. 3.3. With this setup, we can measure the frequency response, determine the Q-factor, and we can study the mode-shapes of both the substrate and resonator. Especially looking at the mode-shape of the measured geometry is a powerful technique not often used in the literature. It is useful to convincingly say which modes are substrate modes and which are resonator modes. Furthermore, it shows where the (anti)nodes of the scanned geometry are when looking at the mode-shape of the substrate.

The trampoline resonators are characterized in the frequency domain with a fiber optic interferometer (MSA-400 Polytec GmbH) at room temperature in a high vacuum (pressure $\leq 1 \times 10^{-5}$ mbar) to minimize viscous damping. The resonator motion was actuated in the linear regime with a piezoelectric shaker (using a pseudo-random signal) and detected with a laser Doppler vibrometer (He-Ne $\lambda = 633$ nm) with a microscope objective of 3x, 5x, and 20x magnification. The signal is decoded by the OFV-5000 vibrometer controller in real-time. The data management system (DMS) is connected to the controller through the junction box, which also provides excitation signals for the piezoelectric shaker. The whole system is placed on a pneumatic damping table (TMC CleanBench), to isolate it from vibrations. The mode-shape can be analyzed with the DMS using the Polytec ScanViewer (PSV).

Furthermore, ring-down measurement (see 2.1.3) in the time-domain to determine the Q-factor can be performed using the same system. First, in the frequency domain, using a pseudo-random signal, the resonance frequency is determined. Then, the resonator is actuated using a sine signal at resonance. The signal is turned off when the steady-state is reached, and in the time domain, the displacement amplitude is measured.

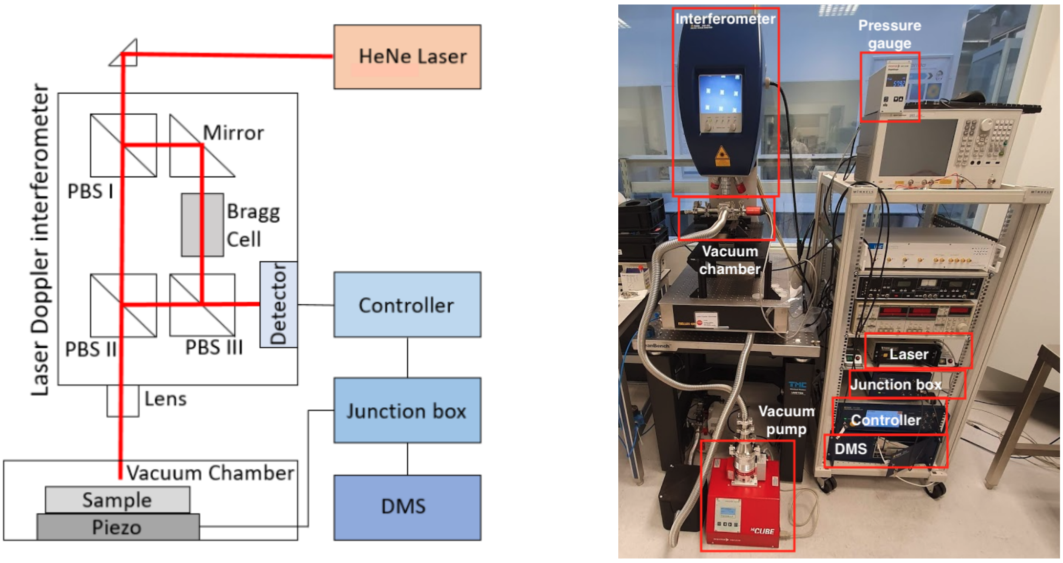
HeNe Laser
Laser Doppler interferometer
Mirror
PBS I
Bragg Cell
Detector
Controller
PBS II
PBS III
Lens
Junction box
Vacuum Chamber
Sample
Piezo
DMS
Interferometer
Pressure gauge
Vacuum chamber
Laser
Junction box
Vacuum pump
Controller
DMS

(A) Schematic of the setup.

(B) Photo of the setup.

FIGURE 3.3: Measurement setup: fiber optic interferometer, the MSA-400 from Polytec GmbH.

3.3 Experimental measurements

To experimentally investigate the influence of mode-coupling on the Q-factor, multiple experiments are done. These experiments are compared to the numerical simulations to see if this model can be used for the design of other resonators. For all experiments, we use high-stress SiN trampoline resonators on top of a silicon substrate, similar to those used in ref. [7]. These structures are easy to measure, and there is a lot of experience within the research group of making these kinds of resonators. Multiple trampoline resonators are fabricated on a single chip, using the fabrication process as discussed in section 2.1.5. This is done to 1) increase the amount of data gathered from one chip and 2) decrease variance between resonators (due to chip thickness, film thickness, etc).

3.3.1 Substrate characterization

The substrate needs to be well characterized in order to do some of the experiments. We have already simulated the substrate to numerically get the eigenfrequencies and mode-shapes. To verify if these numerical simulations represent the reality, we compare them to measured data to check how well the data matches. If the data matches well, we can use this information to design and fabricate chips for other experiments. We fabricate a chip with the same dimensions as in the simulations, and measure the frequency response to determine the eigenfrequency, and resolve the mode-shape to compare this to the simulated data.

3.3.2 Influence of clamping

For now, we expect the resonator to couple to substrate modes. In this experiment we want to investigate the effect of placing the chip on the piezo with different methods, namely: 1) under its own weight, and 2) using double-sided tape, see figure 3.4. We do this to show that we can engineer the Q-factor of resonators by engineering the substrate, in this case reducing the Q-factor of the substrate by taping it down. We can compare the substrate and resonator Q-factors for the two clamping methods. We expect the substrate modes to be much more damped in the case of using double-sided tape and therefore decreasing the Q-factor of the resonator.

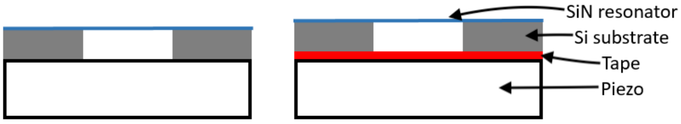

FIGURE 3.4: Placing the chip on the piezo using two clamping methods: 1) under its own weight (left) and 2) using double-sided tape (right).

To investigate this, we fabricate nine trampoline resonators (3x3) on a $10 \times 10\text{mm}^2$ substrate of 500 µm thick. The trampolines are designed to have a resonant frequency of ~328 kHz. The chip is placed on a piezoelectric shaker to drive the resonator. We will measure the frequency response of the resonator and substrate with the two clamping methods, and perform ring-down measurements to determine the Q-factor.

3.3.3 Influence of frequency spacing

In this experiment, we want to combine the gathered information and experimentally measure the influence of frequency spacing on mode-coupling and thereby on the Q-factor. We have characterized a 500 µm thick chip, on which we want to cross one of the substrate modes with the resonator mode. To investigate this, we have fabricated 25 trampoline resonators, see fig. 3.5, in a 5x5 array on a 500 µm thick chip. The trampoline resonators are designed such that each row has a slightly different resonance frequency (± 2.5 kHz), achieved by varying the photonic crystal ratio, see inset fig. 3.5. Our aim is that the middle row will overlap with a substrate mode at 120 kHz. We have identified the substrate mode, and located the nodes and anti-nodes. Since we use a 5x5 array, which spans a large area of the substrate, we can also experimentally verify the mode-shape dependence. We expect that the experimental results show the same behavior as the numerical simulations, that is, resonators which modes are closer to the substrate mode in frequency will show a decrease in Q-factor, and the resonators that lie on a node of the substrate mode-shape will not be affected as much.

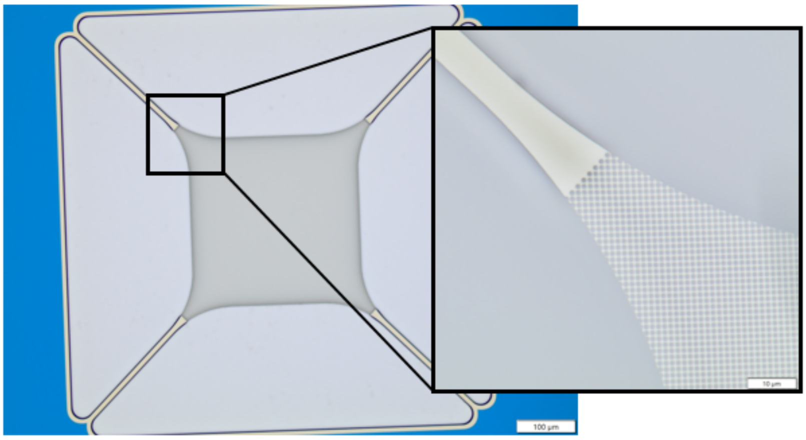

FIGURE 3.5: Example of the trampoline resonator. Inset: Zoom-in of the photonic crystal.

4 Results and discussion

In this chapter, the results of the numerical simulations and experimental measurements are presented. Here we discuss the mode-shape dependence of the coupling between the resonator and substrate modes, furthermore, we look at the influence of substrate thickness and Q-factor of substrate modes on mode-coupling. Next, the results of the experimental measurements are discussed. Two different experiments are done, 1) the chip clamping and 2) the crossing of a substrate mode. The experimental results are compared to those of the simulations to see if the model predicts the behavior of the Q-factor due to mode-coupling.

4.1 Mode-shape dependence

Before we can investigate the mode-coupling to the substrate, we first need to discuss the shape of the substrate modes. In this section, we discuss the results of the mode-shape dependence. First, we characterize the substrate, and then we present the results of the influence of resonator location on the substrate.

4.1.1 Substrate characterization

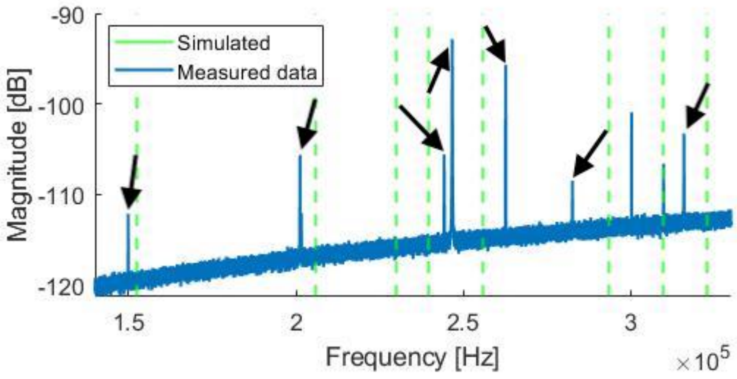

FIGURE 4.1: Simulated (green) eigenfrequencies and measured (blue) frequency response of a 500 µm thick 10x10mm^2 substrate.

In fig. 4.1 we plot the experimental data (blue graph) and the simulated resonance frequencies (green lines) in the frequency range between 140 kHz - 330 kHz (the whole spectrum can be found in the appendix in fig. A.2). The simulations match well with the measured data. We find the correct number of modes, but there are some discrepancies in frequency, which is expected due to the boundary conditions (i.e. chip placement) and fabrication tolerances. The largest frequency mismatch is 15 kHz, which means that, with help of the numerical simulations, we can predict the substrate modes with 90% accuracy. The frequency of the substrate mode is not the only important parameter. All these modes have different shapes, thus we have to check if the mode-shape of the simulated data matches with that of the measured data. We find that the shapes of the different modes match well, three examples are shown in fig. 4.2.

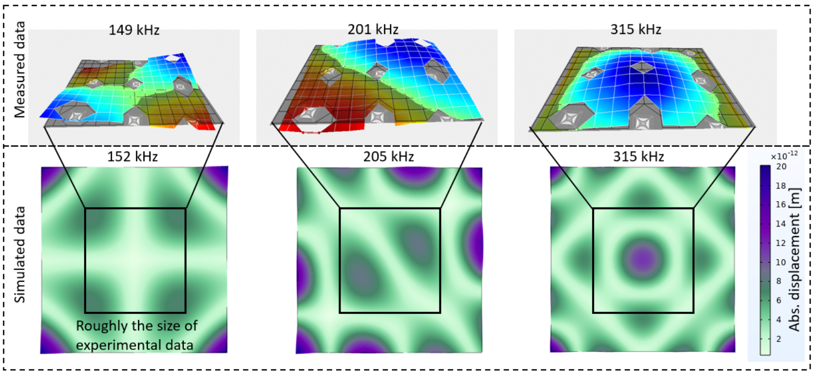

FIGURE 4.2: Measured (top) and simulated (bottom) mode-shapes of the 500 µm thick substrate. Note that the measured mode shape is not the whole substrate, only the center part with the 3x3 array, see fig. A.1 in the appendix.

4.1.2 Nodes and anti-nodes

To investigate the influence of mode-shape on Q-factor we have selected the substrate mode simulated at 292 kHz. This mode has a node at the center of the substrate, and anti-nodes in the four corners (1.8 mm in x and y direction w.r.t. the center). We have plotted the results in fig. 4.3. Each data points represent a simulation with a slightly different mass to sweep the resonance frequency of the resonator. When the resonator is located at an anti-node (fig. 4.3 orange crosses), the resonator mode couples strongly to the substrate mode, which decreases the resonator's Q-factor by several orders of magnitude when the frequency spacing between the two modes is close. On the other hand, when the resonator is located at a node (fig. 4.3 blue crosses), the resonator does not couple (nearly as strong) to this particular mode and only has a minimal effect on the Q-factor when the modes are close in frequency.

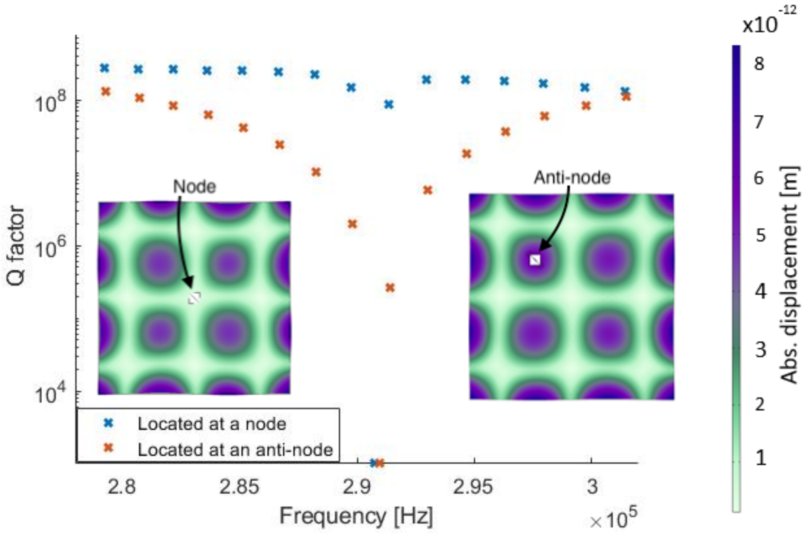

FIGURE 4.3: We simulate the Q-factor of resonators at two locations and find that the mode-shapes of substrate modes are important to consider. This is because when the resonator is located at a node (blue) the mode-coupling and thus effect on the Q-factor is minimal, while at an anti-node (orange) it couples strongly, and the Q-factor decreases several orders of magnitude.

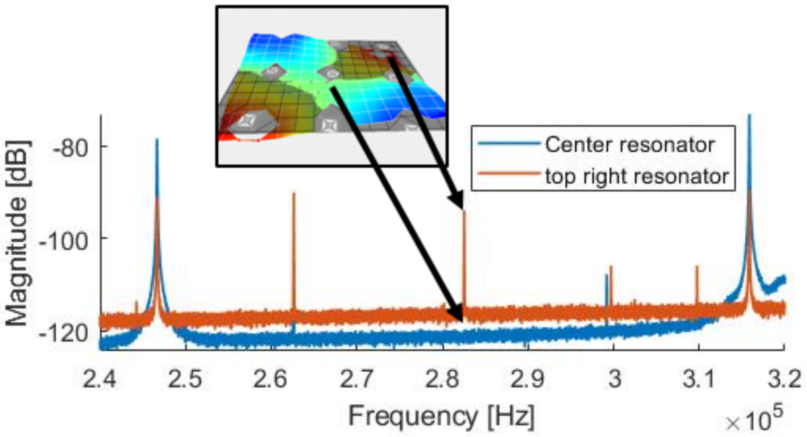

FIGURE 4.4: Frequency response of a corner resonator (orange) and the center resonator (blue). The substrate mode at 282 kHz is only visible in the corner resonator response. Inset: mode-shape of the substrate at 282 kHz.

Thus, we find that when the resonator lies on a node of the mode-shape, it does not couple (as strongly) to that mode, and when it lies on an anti-node, it couples strongly to that mode. This is an important observation because in experiments of high Q resonators it is often the case that multiple resonators are measured on the same chip (i.e. with different locations). This could in general explain many of the variances that many experiments measure with resonators on a chip. If the resonators are located unfavorable with certain modes, there will always be variance in the Q-factor, even if the resonators are designed and made perfectly. This means that correct placement on the chip matters a lot. Furthermore, it can explain why in ref. [26] while crossing substrate modes, the dissipation is not proportional to the measured frame amplitude.

We tested this experimentally by measuring the frequency response of two resonators at the center and corner location of the clamping experiment. In the experiment, the substrate mode is located at 282 kHz instead of 292 kHz, but from the mode-shape measurement, see inset in fig. 4.4, we can see that the corner resonators are located at the anti-nodes of the mode-shape, while the center resonator is located at a node. The frequency response is plotted in fig. 4.4. When we compare the top right corner resonator (orange) with the center (blue) resonator we see that the substrate mode is only visible in the resonator response of the top right, because there is motion amplitude here. Therefore only these (corner) resonators can couple to this mode and experience a decrease in the Q-factor when the modes are close in frequency. For the center resonator, the substrate feels like a fixed boundary.

4.2 Mode-coupling

In this section, we discuss the results of numerical simulations where we try to explain why radiation loss dominates in the findings of ref. [7] and [12]. We investigate the influence of mode-coupling on Q-factor in resonators with different film and substrate thickness, and we also consider differently damped substrates.

4.2.1 Influence film thickness

The results of the simulation for SiN film thickness comparison are plotted in fig. 4.5. The substrate modes are easily recognizable because they have a Q-factor of 10^3. We find that the

20 nm films have roughly a factor five higher Q-factors ($\sim 7.5 \times 10^8$) than those of 100 nm ($\sim 1.5 \times 10^8$), which agrees well with the expected results (considering the first part of equation 1.2 with nominal values and comparing the film thickness t_f).

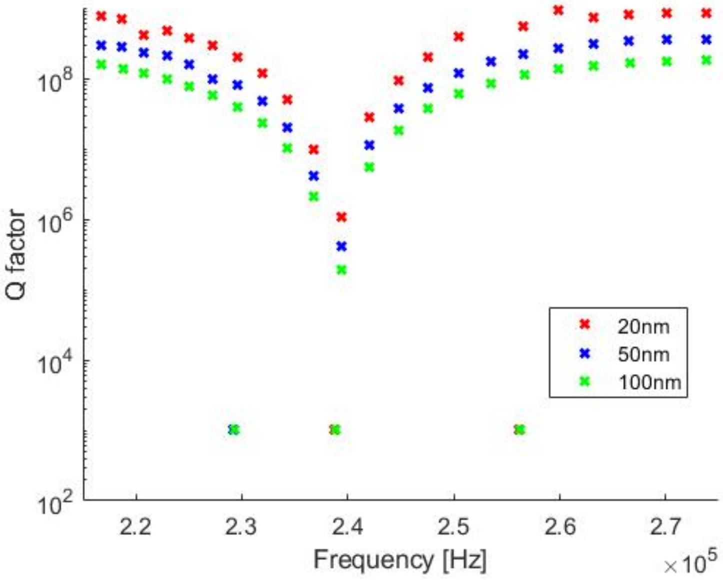

FIGURE 4.5: The simulated Q-factors for substrate and resonator modes with different SiN film thickness.

The resonator is intrinsic loss limited over a wide range of resonance frequencies and in all cases it couples to the substrate mode at 240 kHz, decreasing the Q-factor up to several orders of magnitude. We can thus accept that different film thickness does not affect mode-coupling. Mode-coupling should be visible experimentally in resonators no matter the film thickness ($\leq$100 nm). The effect of mode-coupling is stronger when the difference in the Q-factor is higher (achievable by using very thin resonators). This means that ultra-high Q resonators are much more susceptible for a decrease in the Q-factor due to mode-coupling. It is, therefore, useful to fabricate chips with thin SiN films for experiments, however, very thin films are often difficult to fabricate. Furthermore, with a 5 order difference in the Q-factor between the two modes, the decrease in the Q-factor due to coupling of a resonator mode 20 kHz removed from the substrate mode is negligible.

4.2.2 Influence substrate thickness

The results of the substrate thickness comparison are plotted in fig. 4.6. We have normalized the frequency for the coupled substrate mode to better compare the results. Firstly we find that the thinner substrates couple to the resonator at a larger range of frequencies, i.e. the effect nearby is stronger and the curve is wider. This agrees well with what was found in the analytical calculations, see figure 2.8.

Another important observation is that the resonator on a 200 µm substrate does not reach its intrinsic limit, and is thus limited by radiation loss due to mode-coupling (at least for the simulated frequencies). This is because the resonator couples to multiple modes, which are closer together in frequency spacing with thin substrates ($\omega \propto t$). Since we concluded that mode-coupling happens with all film thickness, this might explain why [7] found that in thin substrates with thin SiN films did not increase in the Q-factor as expected.

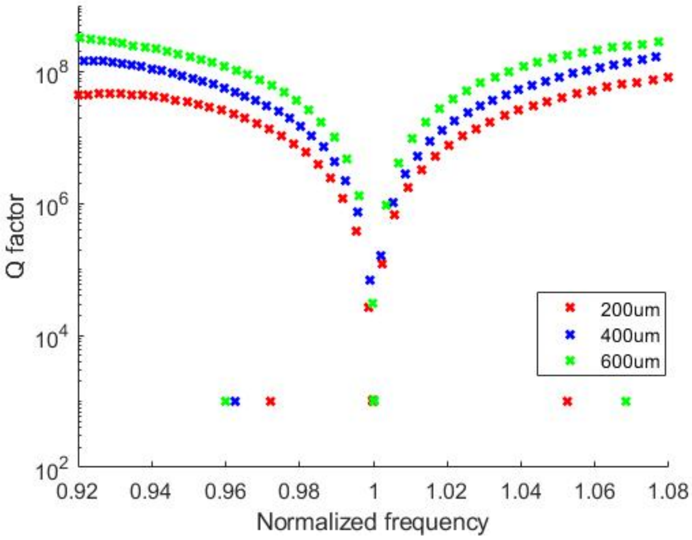

FIGURE 4.6: The simulated Q-factors for substrate and resonator modes with substrates of different thicknesses.

4.2.3 Influence of substrate damping

The results of the differently damped substrates are plotted in fig. 4.7. We have used the values $\eta_s = 10^{-2}$, 10^{-3}, and 10^{-4}. Those result in substrate modes with Q-factors of 10^2, 10^3, and 10^4, respectively, which are reasonable values for substrate modes under different clamping conditions (e.g. free standing and tape the substrate down). From the results, it can be seen that the resonator is limited at a Q-factor of 10^8 and that when the substrate mode has a lower Q-factor, the reduction in the Q-factor is greater compared to the higher Q substrate. This agrees well with our expected results.

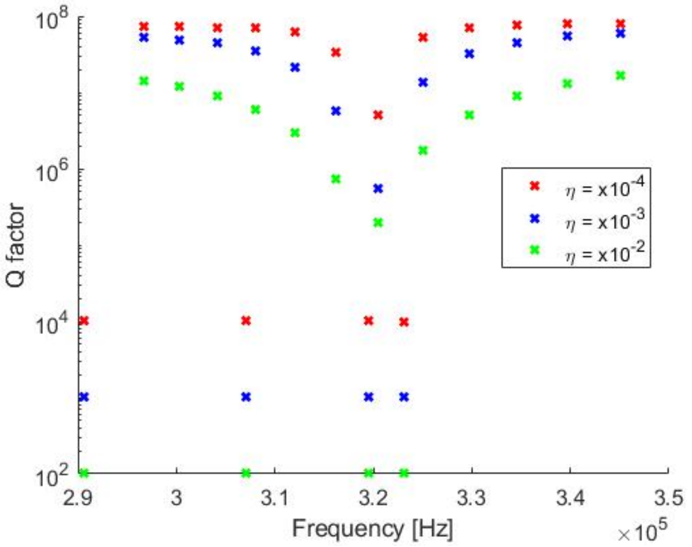

FIGURE 4.7: The simulated Q-factors for substrate and resonator modes with differently damped substrates.

4.3 Experimental: Chip clamping

4.3.1 Influence of tape on Q-factor

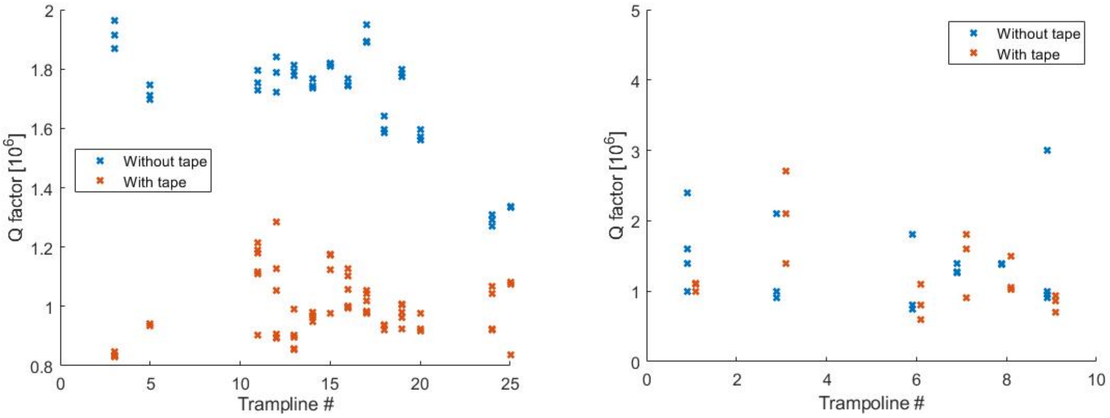

(A) Q-factors of the PhC chip.

(B) Q-factors of the original clamping chip.

FIGURE 4.8: The Q-factors of chips resting under its own weight (blue) and taping the chip down (orange).

We have taped down both chips, that is, the original chip for the clamping experiment and the chip for the frequency spacing (we call this the PhC chip). The Q-factors, determined by the ring-down measurements, are plotted in fig. 4.8. When we compare the Q-factors of the PhC chip, see fig. 4.8a, we can see a clear trend that the Q-factors are reduced by taping it down. The Q-factors of the free chip are approximately 1.8×10^6, while those of the taped down are limited to approximately 1×10^6. Thus we see a decrease of a factor 2 in the Q-factor when the chip is taped down. A decrease in the Q-factor is predicted by the simulations, see section 4.2.3.

However, when we compare the Q-factor of the original chip, see fig. 4.8b, we find that there is no clear trend. We attribute this due to the fact that other loss mechanisms dominate here. These measurements were done in a different vacuum chamber, reaching pressures of just below 1×10^{-5} mbar. Gas damping might limit the Q-factors instead of radiation loss, which will be discussed further in appendix A.5. Furthermore, the substrate mode might be too far away, we will analyze this in the next section.

4.3.2 Analysis of the frequency response

When we compare the taped chip and the chip resting on its own weight, we can see a big difference in the frequency response. We have plotted the results of this experiment in fig. 4.9. The top figure shows the substrate response and the bottom figure shows the resonator response under its own weight (blue), and clamped down with tape (orange), respectively.

The difference in the frequency response is especially noticeable in the original chip, see fig. 4.9b. We find that when the sample is clamped down with double-sided tape, the added losses from the tape drastically reduce the Q-factor of the substrate modes. When we compare this to the expected analytical results we see that it matches well. In the case where the chip rests under its own weight, the substrate modes are visible in the resonator response, while the resonator mode is not visible in the substrate response. When looking at the taped down chip, the substrate modes are reduced to broad peaks, as a result, we also do not see these modes in the resonator response, as expected from the analytical models.

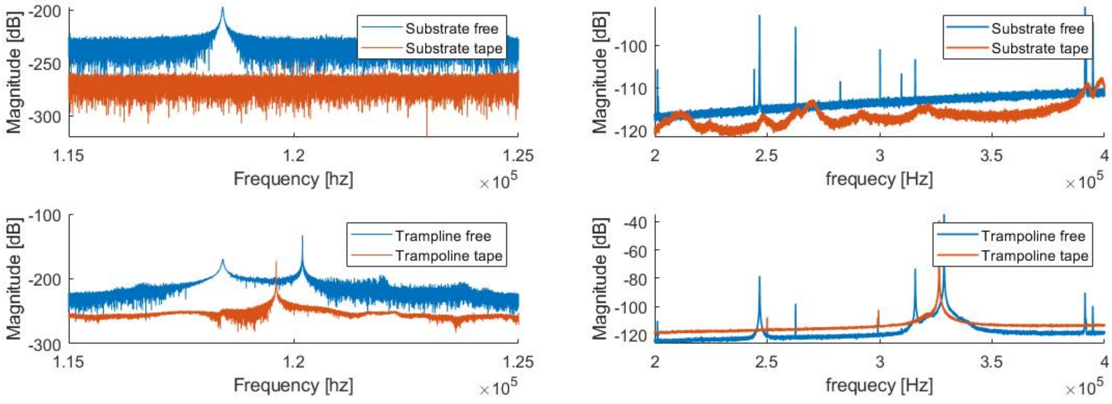

(A) Frequency response of PhC chip.

(B) Frequency response of the clamping chip.

FIGURE 4.9: Frequency response of the substrate (top) and resonator (bottom). We compare the chip resting under its own weight (blue) and taping the chip down (orange).

In the other chip, see fig. 4.9a, the substrates modes are completely buried in the noise floor. This is most likely due to the use of the different vacuum chamber, while it can reach a greater vacuum, the chip driving is very inefficient. Furthermore, because this chip is 1 mm, there are fewer substrate modes compared to the 500 µm thick chip (twice as dense in modes). Therefore, the influence of the tape on the substrate is much more visible in the 500 µm thick chip.

4.3.3 Clamping discussion

The frequency spacing between the resonator mode and the nearest substrate mode in the original clamping chip is 15 kHz, see fig. 4.9b. In the simulations, there is still a decrease in the Q-factor when the modes are 15 kHz removed, but it is not as strong. Furthermore, the uncoupled Q-factor is also 2 orders of magnitude higher (10^8 instead of 10^6). The reason why we did not see a decrease in the Q-factor in this chip can be explained by the fact that the modes are to far apart in combination with the small difference in the Q-factor of the two modes. When we compare this to the PhC chip, which was specially designed to have the modes overlap, there is only 3 kHz between the resonator and substrate mode, and we can clearly see the decrease in the Q-factor. As mentioned before, another explanation might be that we did not have a high enough vacuum, and thus that the resonator is gas damping limited.

In ref. [12] tape was used as clamping and a general trend of a decrease in the Q by a factor of two was found for different width string resonators ($w = 5 - 30\,\mu\text{m}$). This result agrees well with our findings in the taping of the PhC chip, see fig. 4.8a. In their study, a 350 µm thick substrate was used, which results in lots of substrate modes to which the resonator can couple. An experiment that can verify this is, using a 1 mm thick substrate and design a resonator such that it is far away from a substrate mode. When comparing the taped down with a free-standing chip, no difference in the Q-factor would be expected. Lastly, a general trend in a decrease in resonance frequency in the taped down chips was found. This result has not been reported by [12].

4.4 Experimental: frequency spacing

4.4.1 Crossing a substrate mode

From the 25 resonators, 17 were usable, the other 7 either broke or had dust on them. The frequency response of one trampoline resonator for each of the five rows are plotted in fig. 4.10. We can clearly identify the substrate mode at 118.4 kHz, and five different frequencies for the trampoline modes between 116.3 kHz and 121.2 kHz. We note here that each row should have a decrease in resonance frequency of about 2.5 kHz, this was unfortunately not the case. We will discuss this in more detail in the next section.

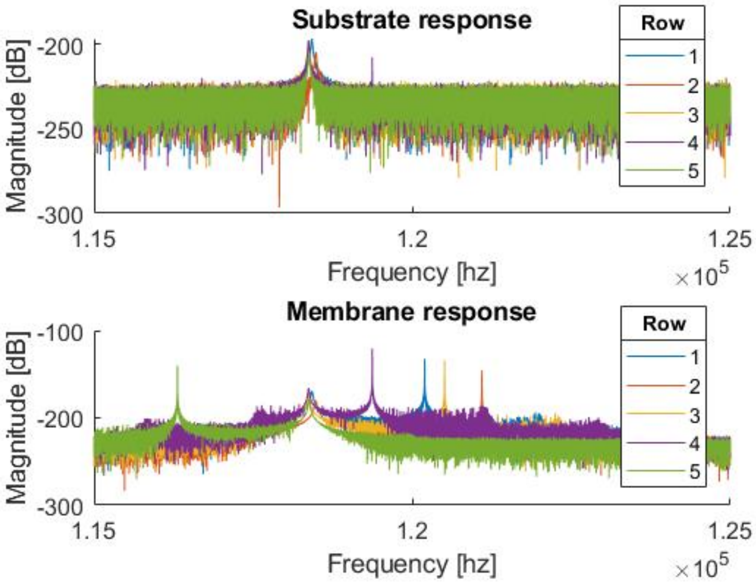

FIGURE 4.10: Frequency response of the substrate (top) and resonators (bottom).

In fig. 4.11a we have plotted the Q-factor from three ring-down measurements for each of the trampolines against the frequency (with the black line being the substrate mode) at the highest available vacuum. The red data points indicate pressures just below 1×10^{-5} mbar, and might still be dominated by gas damping. In fig. 4.11b we present the location data for each of the Q-factors. The bottom row, which all have resonance frequencies lower than that of the substrate mode (<118.4 kHz), have the lowest Q-factors and seem to be limited to $\sim 1.3 \times 10^6$. Furthermore, resonators with frequencies further away seem to first increase in the Q-factor, but then decrease again after ~120 kHz. This is not the expected result, reasons for this will be discussed in the next section..

4.4.2 Frequency spacing discussion

We see a decrease in the Q-factor when the resonator mode is lower in frequency than the substrate mode. The chip was designed such that the trampolines on every row of the 5x5 array had a different resonance frequency, where the third row would overlap with the substrate mode. The data shows that this was not the case. The frequency spacing between the membranes was less than expected. Because of this, only data of -2.1 to +2.8 kHz around the substrate mode could be gathered. We can clearly see a difference in the Q-factor between the bottom row (all resonance frequencies lower in frequency w.r.t. substrate mode) and the

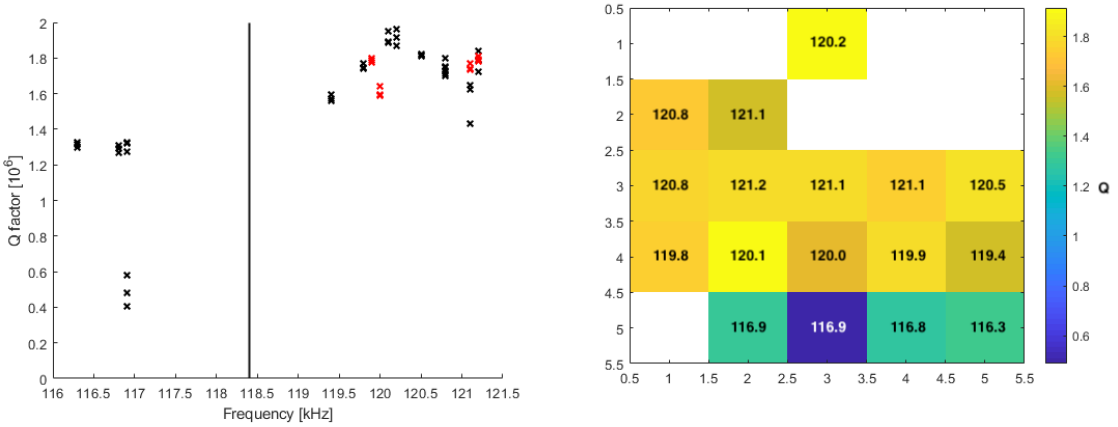

(A) Q-factor vs frequency.

(B) Q-factor vs location (numbers inside squares represent resonance frequency).

FIGURE 4.11: Results of the PhC sweep.

other four rows. Getting the fabrication right for this experiment is something we can still improve on to really see this v-shape seen in the simulations.

Unfortunately, there were some fabrication issues. First of all, a 1 mm thick silicon substrate was used, instead of the designed 500 µm. From the simulations, we have found that with thicker substrates, the effect of mode-coupling on Q-factor is less strong compared to thinner substrates. The increased thickness of the Si substrate in combination with a 100 nm thick SiN film (going much smaller is difficult) might just not be a good enough combination to see the influence of mode-coupling.

Furthermore, due to an issue with the alignment of the dicer, the chip was diced in a trapezoid shape, instead of a square shape. This caused the substrate modes to differ from simulations, fortunately, one substrate mode was still usable to test our hypothesis. We measured the frequency response and mode-shape of the substrate, and simulated a 1 mm thick substrate with approximate dimensions. The mode-shape of the simulation is shown in fig. 4.12, and matches well with the experimental data, see appendix A.6. We can see that there are not really any nodes, thus we can also not compare this.

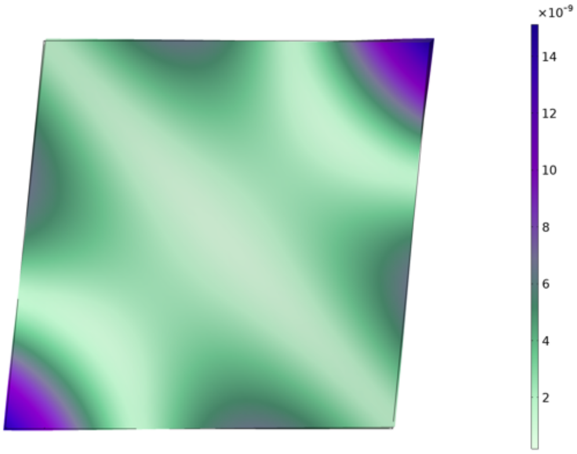

FIGURE 4.12: Simulated mode-shape at 126 kHz.

At least three ring-down measurements were performed for each resonator. Some of the data was measured above 1×10^{-5} mbar, this data was excluded because in this pressure regime the resonators were gas damping limited (all data points can be found in appendix A.7). This can be supported further by the data, where a large increase in the Q-factor was found in general when decreasing the pressure from $>20 \times 10^{-6}$ mbar to 7.3×10^{-6} mbar. When looking at more specific pressures, we find no increase in the Q-factor of resonator 20 when decreasing the pressure from 9.3×10^{-6} mbar to 7.0×10^{-6} mbar, while we do see a slight increase in the Q-factor for resonator 22 when decreasing the pressure from 13×10^{-6} mbar to 7.3×10^{-6} mbar.We note here that we were only able to measure up to 7.0×10^{-6} mbar. Thus, even though the total Q-factor is not dominated by gas damping, it could still play a large role for the higher Q resonators. It is therefore interesting to repeat the experiment in a higher vacuum, i.e. $<1 \times 10^{-6}$ mbar. Furthermore, the membrane with a Q-factor of $\sim 0.5 \times 10^{6}$ was most likely driven at the wrong frequency or had small imperfections causing it to have such low values.

5 Conclusion and Outlook

5.1 Conclusion

In this thesis, we studied the influence of mode-coupling with the substrate on the Q-factor of high-stress SiN resonators. The hypothesis is that the Q-factor can be limited due to mode-coupling with the substrate. This was investigated by analyzing different aspects of the substrate. We can conclude that a resonator mode can couple to a nearby substrate mode and drastically reduce the Q-factor.

The mode-shape of the substrate mode is important to consider, because coupling with the substrate mode only happens at anti-node locations, where the relative motion amplitude of the mode is high, that is, motion in the same direction. On the other hand, nodes of the mode-shape do not couple with the resonator. Experimentally this has been shown to be the case because substrate modes do not appear in the response of resonators located at nodes.

Furthermore, the frequency spacing between the resonator and substrate mode is important, because substrate modes close in frequency w.r.t. the resonator mode can couple and exchange energy. Since the substrate modes have a relatively low Q-factor, energy is lost faster in these modes. This means that if a resonator mode couples to a substrate mode, energy is lost through the substrate and, therefore, reduces the Q-factor. The closer these modes are in frequency, the stronger the coupling and a greater reduction in the Q-factor. When the modes overlap, the Q-factor of the hybridized mode is significantly reduced. Thinner substrates have a higher density of modes, this means that there are more potential substrate modes to couple with, and can even limit the Q-factor in ultra-high Q resonators.

Lastly, we have investigated the influence of clamping the substrate down with tape. We conclude that tape drastically reduces the Q-factor of substrate modes. As a result, resonator modes that couple have a decreased Q-factor. This means that using any form of clamping is not recommended, but instead use the chip free standing.

Our results demonstrate that the substrate choice, as it can strongly affect the Q-factor of resonators, should become an integral part of the resonator design phase. In most real applications we need to clamp down the chip in some way. This theoretical framework allows us the possibility to design our resonators so that we get minimal influence from substrates that realistically need to be clamped down for stability in real sensor applications. Also, it allows us to understand that, even if our resonator fabrication is perfect, we can still get variance in their performance just by where the resonators are placed on a substrate.

This research is important for ultra-high Q resonators because these are very sensitive to extra energy loss. In this study, we used resonators with a Q-factor of order 10^6, while the state of the art achieve Q-factors of over 10^8. With these ultra-high Q-factors, the substrate becomes more and more important to consider, because it can be the limiting factor. Eventually, resonators that do not use a phononic shield, have to consider the substrate when radiation loss starts to dominate. When using thick and freestanding substrates, the influence of mode-coupling can be decreased. Furthermore, when taking into account the resonance frequencies and mode-shape of the substrate, this effect can be further reduced. These results can be used with minimal changes in the fabrications method, and can enhance the Q-factor of devices without increase in device size.

5.2 Recommendations and outlook

For further research, it would be an added value to look further into the mode-coupling while crossing a substrate mode. In this project, we were not completely successful in achieving the range of frequencies we had planned. Using the photonic crystal to achieve the frequency range looks promising, but the correct method for fabrication needs to be investigated. Repeating the experiment with the new knowledge of mode-shape dependence, a greater understanding can be formed. This can be combined with a comparison of placing resonators on both nodes and anti-nodes.

The model presented in this thesis explains the behavior well, but further research needs to be done to find the correct parameters to accurately predict Q-factors. In our model, we have fitted the structural loss parameters such that a Q-factor of approximately 10^8 was achieved when the modes did not couple, however, how to accurately model this loss mechanism is unknown. To calculate the Q-factor for intrinsic loss, the energy in tension and bending can be computed using FEM software, but this does not take into account the substrate. We have thought of ways to expand this to include the substrate, but have not succeeded as of yet and could be valuable future research.

Furthermore, some time was spend on investigating the influence of the overhang on the Q-factor. In some studies, the overhang can be quite significant and can be regarded as an intermediate substrate. The overhang can have its own set of resonance frequencies, and the Q-factor will have dropped since it is not under the high stress that the resonator experiences. The exact role it plays remains unknown.

A Appendix

A.1 Nominal values for trampoline resonator

In table A.1 the nominal values for the trampoline resonator are presented.

Parameter	value
Si chip thickness	500 µm
SiN film thickness	50 nm
Tether width	10 µm
Outer fillet radius	20 µm
Inner fillet radius	100 µm
membrane width	200 µm
Initial stress	1 GPa
Overhang size	10 µm
Window width	700 µm
Substrate width	10 mm × 10 mm
PhC Ratio	0.4

TABLE A.1: Nominal values for trampoline resonator design parameter.

A.2 Results of parameter sweep on resonance frequency

In table A.2 the results of the resonance frequencies from the parameter sweep are presented.

Outer fillet $[10^{-6}\,\mathrm{m}]$	freq [kHz]	Membrane size $[10^{-6}\,\mathrm{m}]$	freq [kHz]	Tether width $[10^{-6}\,\mathrm{m}]$	freq [kHz]	PhC ratio	freq [kHz]
5	159	60	220	10	151	0.4	161
10	162	80	190	15	179	0.45	155
15	165	100	169	20	202	0.5	150
20	169	120	150	25	220	0.55	145
25	172	140	135	30	233	0.6	141
30	176	160	125	35	246	0.65	137
35	180	180	116	40	256	0.7	133
40	185	200	108	45	265	0.75	130
45	189	220	102	50	275	0.8	127
50	194	240	98	55	281	0.85	125
		250	95	60	290	0.9	121

TABLE A.2: Different parameter sweeps and their effect on the resonance frequency.

A.3 Sample in vacuum chamber

In fig. A.1, a photo of the vacuum chamber with a chip is shown. The chip was used to compare the mode-shape of the simulations with experimental data. Even lowest magnification could not capture the whole chip. In this figure we show the ratio between measured data and the whole chip (see section 4.1.1).

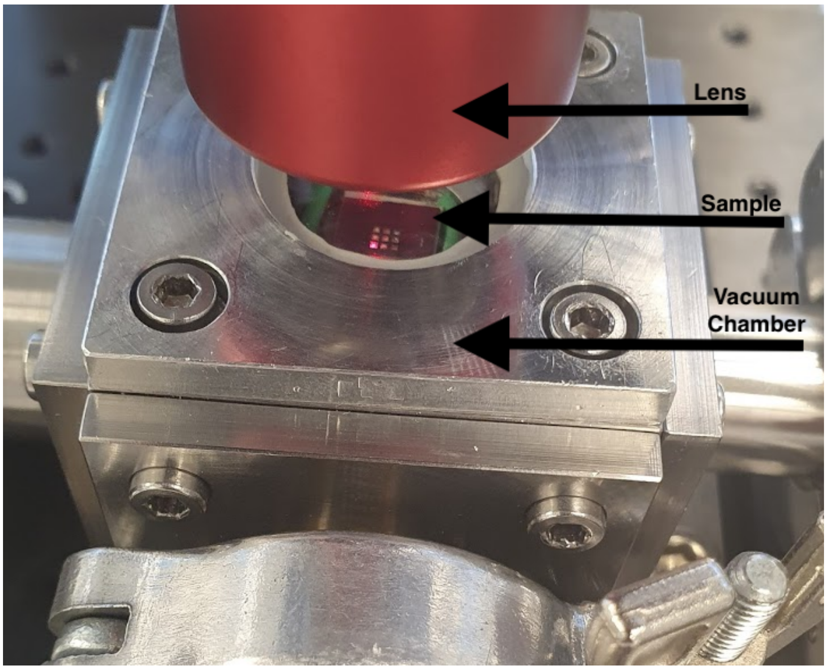

FIGURE A.1: The polytec is not able to capture the whole chip in one measurement due to the magnification of the lens. When looking at the mode-shape the placement of the 3x3 array can be used to estimate the scale.

A.4 Substrate frequency comparison

We compared the simulated and measured resonance frequencies. In fig. A.2 we show the data from 0 to 500 kHz. Furthermore, we also show a zoom-in of two modes very close in frequency, to show that these are predicted as well, see fig. A.3.

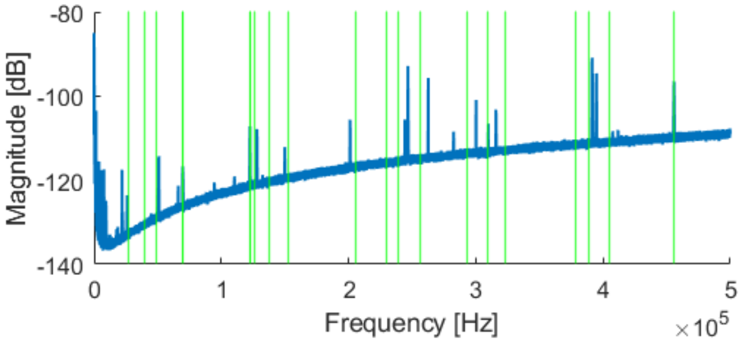

FIGURE A.2: Total measured spectrum (blue) of a 500 µm thick substrate. The green lines are the eigenfrequencies of a simulated 500 µm thick substrate.

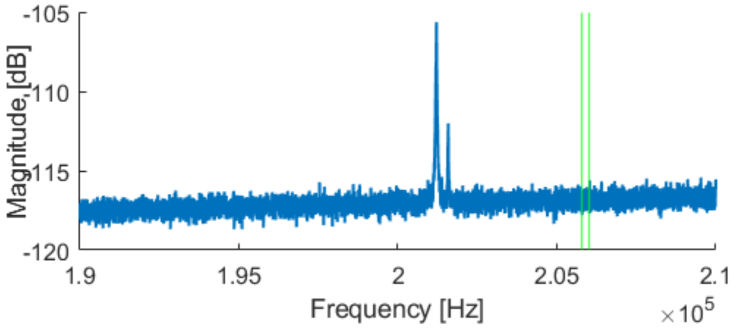

FIGURE A.3: A zoom-in of the measured spectrum (blue) of a 500 µm thick substrate, where we measure two modes, which is also predicted by simulations (green lines).

A.5 Gas damping limited Q-factor

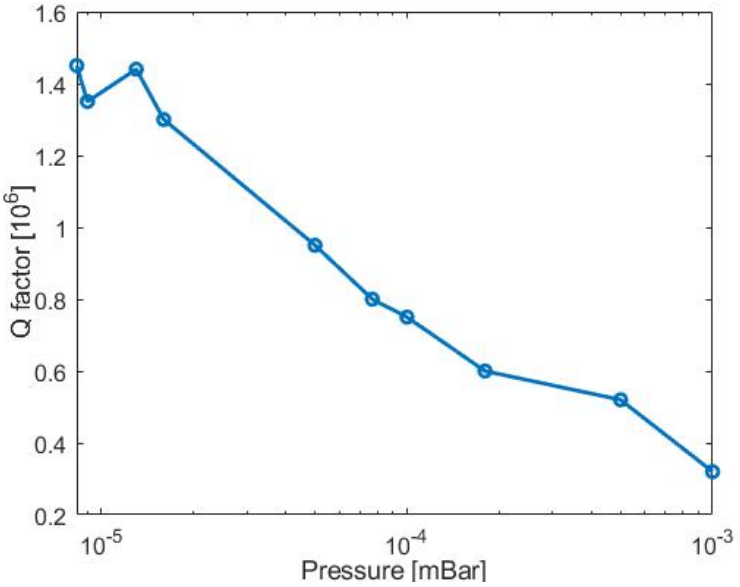

FIGURE A.4: Q-factors limited by pressure.

We know that the total Q-factor is calculated as $\frac{1}{Q_{total}} = \frac{1}{Q_{viscous}} + \frac{1}{Q_{bending}} + \frac{1}{Q_{TED}} + \frac{1}{Q_{radiation}}$ were TED was negligible by using high-stress SiN and gas damping was negligible by using a high enough vacuum. Before we can conclude if the other dissipation mechanisms dominate the Q-factor needs to be measured while decreasing the pressure, when decreasing the pressure does not change the Q-factor anymore we can accept that gas damping is negligible.

In the molecular region, meaning the damping is caused by independent collisions of non-interacting air molecules with the moving surface of the resonator, the Q-factor is given by [19]

$$Q_{viscous} = \frac{\rho t \omega}{4} \sqrt{\frac{\pi}{2}} \sqrt{\frac{RT}{M}} \frac{1}{P} \tag{A.1}$$

where ω is the resonance frequency, t is the resonator thickness, ρ is the density of the resonator, P is the pressure, R is the gas constant, T is the temperature$M$ is molar mass of the gas. At a pressure of 1×10^{-5} mbar the Q-factor should be $>10^8$, which is greater than the intrinsic limit of our resonators, and thus this pressure should satisfy.

The results of this experiment are plotted in fig. A.4. We find that the Q-factor increases until a pressure of roughly 1×10^{-5} mbar, after which it stabilizes around a Q-factor of 1.4×10^6. Our vacuum pump was able to reach this pressure after half a day of pumping. This limited the time we could do reliable experiments.We note here that at a pressure of 1×10^{-4} mbar the Q-factor considering only gas damping is $>10^7$, while we can clearly see it is still increasing in the Q-factor. Our pressure sensor was directly attached to the vacuum chamber, so it is unlikely it was giving a very different value. Therefore, we suspect that this equation cannot be directly used for trampoline structures.

A.6 Mode-shape of the PhC chip

In fig. A.5 we plot the maximal substrate amplitude on the location of the resonators. The diagonal shape is also seen in the simulated mode-shape (see section 4.4.2) and the measured mode-shape, see fig. A.6.

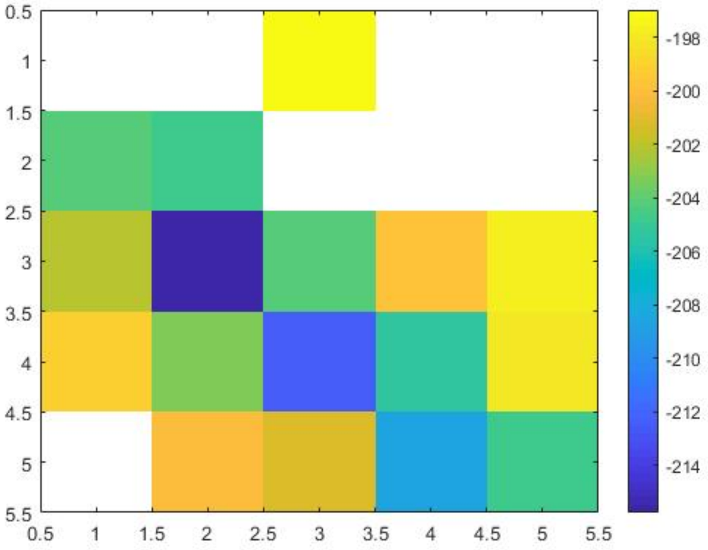

FIGURE A.5: Magnitude of the substrate response per resonator.

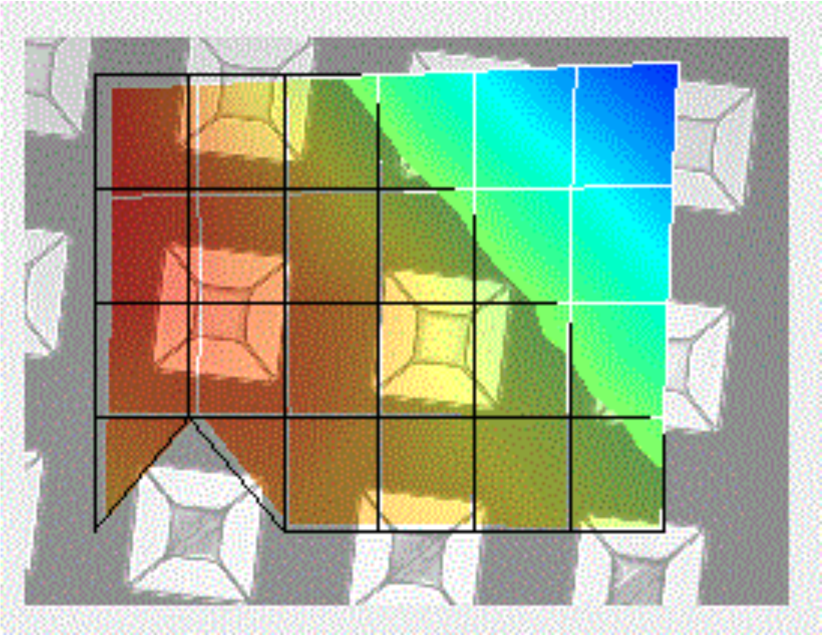

FIGURE A.6: Measured mode-shape of the 1 mm thick substrate.

A.7 Q-factors of the PhC chip

all Q-factors of the ring-down measurement from the PhC Sweep experiment.

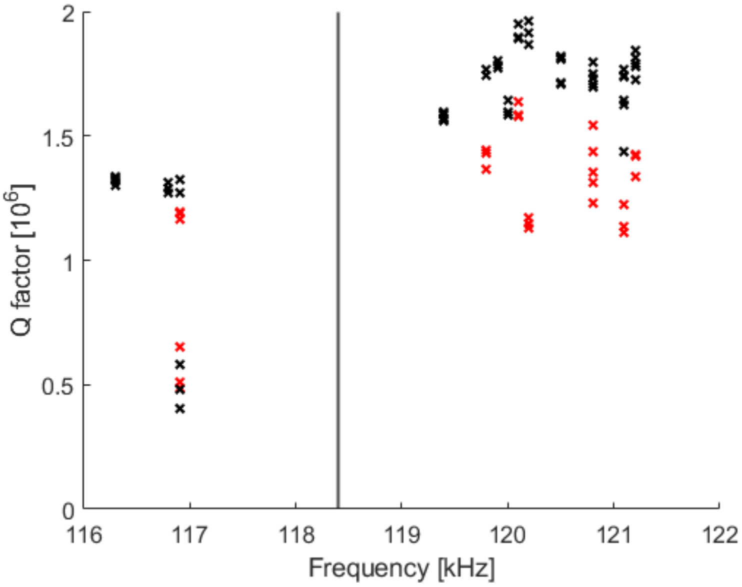

FIGURE A.7: All Q-factors from the ring-down measurement in the frequency spacing chip. The red crosses are measured at a pressure >1 × 10^{-5} mbar

Bibliography

[1] J. Chan, T. P. M. Alegre, A. H. Safavi-Naeini, J. T. Hill, A. Krause, S. Gröblacher, M. Aspelmeyer, and O. Painter, “Laser cooling of a nanomechanical oscillator into its quantum ground state,” *Nature*, vol. 478, no. 89–92, 7367 2011, ISSN: 1476-4687. DOI: 10.1038/nature10461.

[2] J. D. Teufel, T. Donner, D. Li, J. W. Harlow, M. S. Allman, K. Cicak, A. J. Sirois, J. D. Whittaker, K. W. Lehnert, and R. W. Simmonds, “Sideband cooling of micromechanical motion to the quantum ground state,” *Nature*, vol. 475, pp. 359–363, 7356 2011, ISSN: 1476-4687. DOI: 10.1038/nature10261.

[3] K. Jensen, K. Kim, and A. Zettl, “An atomic-resolution nanomechanical mass sensor,” *Nature Nanotechnology*, vol. 3, pp. 533–537, 9 2008, ISSN: 1748-3395. DOI: 10.1038/nnano.2008.200.

[4] B. Ilic, H. G. Craighead, S. Krylov, W. Senaratne, C. Ober, and P. Neuzil, “Attogram detection using nanoelectromechanical oscillators,” *Journal of Applied Physics*, vol. 95, no. 7, pp. 3694–3703, 2004. DOI: 10.1063/1.1650542.

[5] R. P. Feynman, R. B. Leighton, and M. Sands, *The Feynman Lectures on Physics*. 1964.

[6] Jinling Yang, T. Ono, and M. Esashi, “Energy dissipation in submicrometer thick single-crystal silicon cantilevers,” *Journal of Microelectromechanical Systems*, vol. 11, no. 6, pp. 775–783, 2002.

[7] R. A. Norte, J. P. Moura, and S. Gröblacher, “Mechanical resonators for quantum optomechanics experiments at room temperature,” *Phys. Rev. Lett.*, vol. 116, p. 147 202, 14 2016. DOI: 10.1103/PhysRevLett.116.147202.

[8] M. Aspelmeyer, T. J. Kippenberg, and F. Marquardt, “Cavity optomechanics,” *Rev. Mod. Phys.*, vol. 86, pp. 1391–1452, 4 2014. DOI: 10.1103/RevModPhys.86.1391.

[9] D. Rugar, R. Budakian, H. J. Mamin, and B. W. Chui, “Single spin detection by magnetic resonance force microscopy,” *Nature*, vol. 430, pp. 329–332, 6997 2004, ISSN: 1476-4687. DOI: 10.1038/nature02658.

[10] H. J. Mamin and D. Rugar, “Sub-attonewton force detection at millikelvin temperatures,” *Applied Physics Letters*, vol. 79, no. 20, pp. 3358–3360, 2001. DOI: 10.1063/1.1418256.

[11] S. S. Verbridge, J. M. Parpia, R. B. Reichenbach, L. M. Bellan, and H. G. Craighead, “High quality factor resonance at room temperature with nanostrings under high tensile stress,” *Journal of Applied Physics*, vol. 99, no. 12, p. 124 304, 2006. DOI: 10.1063/1.2204829.

[12] S. Schmid, K. D. Jensen, K. H. Nielsen, and A. Boisen, “Damping mechanisms in high-q micro and nanomechanical string resonators,” *Phys. Rev. B*, vol. 84, p. 165 307, 16 2011. DOI: 10.1103/PhysRevB.84.165307.

[13] S. A. Fedorov, N. J. Engelsen, A. H. Ghadimi, M. J. Bereyhi, R. Schilling, D. J. Wilson, and T. J. Kippenberg, “Generalized dissipation dilution in strained mechanical resonators,” *Phys. Rev. B*, vol. 99, p. 054 107, 5 2019. DOI: 10.1103/PhysRevB.99.054107.

[14] A. H. Ghadimi, S. A. Fedorov, N. J. Engelsen, M. J. Bereyhi, R. Schilling, D. J. Wilson, and T. J. Kippenberg, *Strain engineering for ultra-coherent nanomechanical oscillators*, 2017. arXiv: 1711.06247 [cond-mat.mes-hall].

[15] A. H. Ghadimi, D. J. Wilson, and T. J. Kippenberg, "Radiation and internal loss engineering of high-stress silicon nitride nanobeams," *Nano Letters*, vol. 17, no. 6, pp. 3501–3505, 2017. DOI: `10.1021/acs.nanolett.7b00573`.

[16] Y. Tsaturyan, A. Barg, E. Polzik, and A. Schliesser, "Ultracoherent nanomechanical resonators via soft clamping and dissipation dilution," *Nature Nanotech*, vol. 12, 776–783, 2017. DOI: `https://doi-org.tudelft.idm.oclc.org/10.1038/nnano.2017.101`.

[17] A. H. Ghadimi, S. A. Fedorov, N. J. Engelsen, M. J. Bereyhi, R. Schilling, D. J. Wilson, and T. J. Kippenberg, "Elastic strain engineering for ultralow mechanical dissipation," *Science*, vol. 360, no. 6390, pp. 764–768, 2018, ISSN: 0036-8075. DOI: `10.1126/science.aar6939`.

[18] M. J. Bereyhi, A. Beccari, S. A. Fedorov, A. H. Ghadimi, R. Schilling, D. J. Wilson, N. J. Engelsen, and T. J. Kippenberg, "Clamp-tapering increases the quality factor of stressed nanobeams," *Nano Letters*, vol. 19, no. 4, pp. 2329–2333, 2019. DOI: `10.1021/acs.nanolett.8b04942`.

[19] S. S. Verbridge, H. G. Craighead, and J. M. Parpia, "A megahertz nanomechanical resonator with room temperature quality factor over a million," *Applied Physics Letters*, vol. 92, no. 1, p. 013 112, 2008. DOI: `10.1063/1.2822406`.

[20] S. Chakram, Y. S. Patil, L. Chang, and M. Vengalattore, "Dissipation in ultrahigh quality factor sin membrane resonators," *Phys. Rev. Lett.*, vol. 112, p. 127 201, 12 2014. DOI: `10.1103/PhysRevLett.112.127201`.

[21] C. Reinhardt, T. Müller, A. Bourassa, and J. C. Sankey, "Ultralow-noise sin trampoline resonators for sensing and optomechanics," *Phys. Rev. X*, vol. 6, p. 021 001, 2 2016. DOI: `10.1103/PhysRevX.6.021001`.

[22] D. W. Carr, S. Evoy, L. Sekaric, H. G. Craighead, and J. M. Parpia, "Measurement of mechanical resonance and losses in nanometer scale silicon wires," *Applied Physics Letters*, vol. 75, no. 7, pp. 920–922, 1999. DOI: `10.1063/1.124554`.

[23] D. M. Photiadis and J. A. Judge, "Attachment losses of high q oscillators," *Applied Physics Letters*, vol. 85, no. 3, pp. 482–484, 2004. DOI: `10.1063/1.1773928`.

[24] J. A. Judge, D. M. Photiadis, J. F. Vignola, B. H. Houston, and J. Jarzynski, "Attachment loss of micromechanical and nanomechanical resonators in the limits of thick and thin support structures," *Journal of Applied Physics*, vol. 101, no. 1, p. 013 521, 2007. DOI: `10.1063/1.2401271`.

[25] I. Wilson-Rae, R. A. Barton, S. S. Verbridge, D. R. Southworth, B. Ilic, H. G. Craighead, and J. M. Parpia, "High-q nanomechanics via destructive interference of elastic waves," *Phys. Rev. Lett.*, vol. 106, p. 047 205, 4 2011. DOI: `10.1103/PhysRevLett.106.047205`.

[26] A. Jöckel, M. T. Rakher, M. Korppi, S. Camerer, D. Hunger, M. Mader, and P. Treutlein, "Spectroscopy of mechanical dissipation in micro-mechanical membranes," *Applied Physics Letters*, vol. 99, no. 14, p. 143 109, 2011. DOI: `10.1063/1.3646914`.

[27] D. J. Wilson, "Cavity optomechanics with high stress silicon nitride films," Ph.D. California Institute of Technology, 2012. DOI: `10.7907/VB3C-1G76`.

[28] Y.-H. Park and K. Park, "High-fidelity modeling of mems resonators. part i. anchor loss mechanisms through substrate," *Journal of Microelectromechanical Systems*, vol. 13, no. 2, pp. 238–247, 2004. DOI: `10.1109/JMEMS.2004.825300`.

[29] D. S. Bindel and S. Govindjee, "Elastic pmls for resonator anchor loss simulation," *International Journal for Numerical Methods in Engineering*, vol. 64, no. 6, pp. 789–818, 2005. DOI: `https://doi.org/10.1002/nme.1394`.

[30] A. Darvishian, B. Shiari, G. He, and K. Najafi, "Effect of substrate thickness on quality factor of mechanical resonators," in *2015 IEEE International Symposium on Inertial Sensors and Systems (ISISS) Proceedings*, 2015, pp. 1–4.

[31] I. Wilson-Rae, “Intrinsic dissipation in nanomechanical resonators due to phonon tunneling,” *Phys. Rev. B*, vol. 77, p. 245 418, 24 2008. DOI: `10.1103/PhysRevB.77.245418`.

[32] G. D. Cole, I. Wilson-Rae, K. Werbach, M. R. Vanner, and M. Aspelmeyer, “Phonon-tunnelling dissipation in mechanical resonators,” *Nature Communications*, vol. 2, 1 2011. DOI: `10.1038/ncomms1212`.

[33] A. N. Cleland and M. L. Roukes, “Noise processes in nanomechanical resonators,” *Journal of Applied Physics*, vol. 92, no. 5, pp. 2758–2769, 2002. DOI: `10.1063/1.1499745`.

[34] P. Steeneken, J. Ruigrok, S Kang, J. van Beek, J Bontemps, and J.-J. Koning, “Parameter extraction and support-loss in mems resonators,” *Proc. Comsol conference 2007, https://arxiv.org/abs/1304.7953*, p. 725, Oct. 2007.

[35] K. Y. Yasumura, T. D. Stowe, E. M. Chow, T. Pfafman, T. W. Kenny, B. C. Stipe, and D. Rugar, “Quality factors in micron- and submicron-thick cantilevers,” *Journal of Microelectromechanical Systems*, vol. 9, no. 1, pp. 117–125, 2000. DOI: `10.1109/84.825786`.

[36] M. Weinberg, R. Candler, S. Chandorkar, J. Varsanik, T. Kenny, and A. Duwel1, “Energy loss in mems resonators and the impact on inertial and rf devices,” in *TRANSDUCERS 2009 - 2009 International Solid-State Sensors, Actuators and Microsystems Conference*, 2009, pp. 688–695.

[37] S. Joshi, S. Hung, and S. Vengallatore, “Design strategies for controlling damping in micromechanical and nanomechanical resonators,” *EPJ Techniques and Instrumentation*, vol. 1, pp. 5–19, 1 2014, ISSN: 2195-7045. DOI: `10.1186/epjti5`.

[38] (). “Nanomechanical resonator,” [Online]. Available: `https://www.wikiwand.com/en/Nanomechanical_resonator`.

[39] R. N. Candler, A. Duwel, M. Varghese, S. A. Chandorkar, M. A. Hopcroft, Woo-Tae Park, Bongsang Kim, G. Yama, A. Partridge, M. Lutz, and T. W. Kenny, “Impact of geometry on thermoelastic dissipation in micromechanical resonant beams,” *Journal of Microelectromechanical Systems*, vol. 15, no. 4, pp. 927–934, 2006. DOI: `10.1109/JMEMS.2006.879374`.

[40] F. R. Blom, S. Bouwstra, M. Elwenspoek, and J. H. J. Fluitman, “Dependence of the quality factor of micromachined silicon beam resonators on pressure and geometry,” *Journal of Vacuum Science & Technology B: Microelectronics and Nanometer Structures Processing, Measurement, and Phenomena*, vol. 10, no. 1, pp. 19–26, 1992. DOI: `10.1116/1.586300`.

[41] W. Gao, F. Wang, and O. Sigmund, “Systematic design of high-q prestressed micro membrane resonators,” *Computer Methods in Applied Mechanics and Engineering*, vol. 361, p. 112 692, 2020, ISSN: 0045-7825. DOI: `https://doi.org/10.1016/j.cma.2019.112692`.

[42] D. Chang, “Thermoelastic damping in thin plates and membranes,” 2010.

[43] S. C. Sundar, “Dissipation and nonlinear mechanics in ultrahigh quality factor membrane resonators,” Doctor of Philosophy, Cornell University, 2015.

[44] E. Romero Sanchez, “Phononics: Engineering and control of acoustic fields on a chip,” Doctor of Philosophy, The University of Queensland, May 10, 2019.

[45] C. markus Gartner, “Advanced membrane architectures for multimode opto-mechanics,” Dpctoral thesis, Wien University.

[46] M. de Jong, *Private communication with ir. m.h.j. de jong about the comsol model*, 2020.

[47] P. Sadeghi, M. Tanzer, S. L. Christensen, and S. Schmid, “Influence of clamp-widening on the quality factor of nanomechanical silicon nitride resonators,” *Journal of Applied Physics*, vol. 126, no. 16, p. 165 108, 2019. DOI: `10.1063/1.5111712`.